Apical oxygen ions and the electronic structure of the high-T_c cuprates

L. F. Feiner
Philips Research Laboratories, P.O. Box 80000, 5600 JA Eindhoven, The Netherlands

M. Grilli and C. Di Castro
Dipartimento di Fisica, Università "La Sapienza," Piazzale A. Moro 2, 00185 Roma, Italy,
(Received 2 October 1991)

We analyze a five-band extended Hubbard model involving four orbitals on the CuO_2 planes of the high-temperature superconducting oxides ($d_{x^2-y^2}$ and $d_{3z^2-r^2}$ for the copper, and $2p_x$ and $2p_y$ for the oxygen) and the $2p_z$ orbital(s) for the out-of-plane apical oxygen ion(s). The strong local repulsion between holes on copper is treated by means of a slave-boson approach in mean-field approximation, whereas the nearest-neighbor Cu-O Coulombic repulsion is treated within a Hartree decoupling scheme. We systematically investigate the variation of the resulting band structure with doping and with varying model parameters, and examine its stability with respect to lattice deformations. The results are compared with experimental data on photoemission, polarized x-ray-absorption spectroscopy, electron-energy-loss spectroscopy, and optical absorption. We analyze in particular the effects of the apical oxygen(s) on the electronic structure, and we identify the amount n_{a_1} of holes in states with local a_1 symmetry as the quantity most directly affected by their presence. This quantity differentiates between the various high-T_c cuprates, which are otherwise very similar as far as the planar structure is concerned. An analysis of ten different classes of compounds reveals a correlation between the maximum critical temperature $T_c^{\max}$ attained within each class at the optimum doping $\delta^{\max}$ and the excess of a_1 holes with respect to the doping itself $n_{a_1}(\delta^{\max})-\delta^{\max}$. This correlation indicates that the highest critical temperature can be reached in the compounds where the interaction between apical oxygen(s) and CuO_2 plane is weakest. We discuss some implications of our results in the light of various theoretical models.

I. INTRODUCTION

Although the enormous theoretical and experimental effort[1] has led to important general insights into the chemical and electronic structure of the high-T_c cuprates,[2] a satisfactory understanding of the phenomenon of high-temperature superconductivity and of its occurrence in the copper oxides is still far from being achieved. Of course, there is now general agreement that the CuO_2 planes common to all the high-T_c compounds, are the crucial structural element. Furthermore, it has become clear from electron spectroscopy that the undoped high-T_c oxides are charge-transfer insulators. The single hole per unit cell is predominantly in the $d_{x^2-y^2}$ (d_x) orbital of the copper ion in the CuO_2 plane, but this is considerably hybridized with the $p\sigma$ orbitals on the surrounding oxygen ions. Electrons added by n doping therefore occupy orbitals of predominantly copper character, but extra holes introduced by p doping have been shown[3,4] to go into states with a large amplitude on oxygen. This is the most direct evidence for the existence of strong correlations between the electrons due to the strong Coulomb repulsion ($U=8-10$ eV) between holes on copper. This feature makes the theoretical treatment of these systems difficult so that, at present, even the Fermi-liquid or non-Fermi-liquid nature of the normal (nonsuperconducting) state is debated.

A major theoretical challenge is therefore to find the simplest model for the holes in the CuO_2 planes that still contains all the essential aspects of the low-energy physics relevant for superconductivity. In this respect the three-band extended Hubbard model[5] that includes the copper d_x orbital and the oxygen $p\sigma$ orbitals in the plane, has been the starting point for many further developments. Having as ingredients copper-oxygen charge-transfer gap, copper-oxygen hopping, and Coulomb repulsion on copper, the three-band extended Hubbard model is constructed to capture both the strong copper-oxygen hybridization and the strong correlations on the copper ions. Through superexchange it gives rise to antiferromagnetism which might provide the mechanisms for high-T_c superconductivity. If amended to include nearest-neighbor Coulomb repulsion between holes on copper and on oxygen, it contains charge-transfer excitons which have been suggested as an alternative mechanism.[6]

When we consider the three-band model as a reference point, both the possibility for further simplification and the necessity of further extension have been advocated. On the one side is the proposal that the model can be reduced to an effective single-band model. Zhang and Rice[7] pointed out that, at finite doping, a hole in a d_x orbital and a hole on planar oxygen in the molecular orbital combination of local b_1 symmetry $\frac{1}{2}(p_{x_1}-p_{y_2}-p_{x_3}+p_{y_4})$ could form a local singlet (for the choice of the phase convention of the orbitals see Fig. 1). More detailed impurity and cluster calculations[8-10] showed that, for realistic parameters, such singlets are likely to be sufficiently

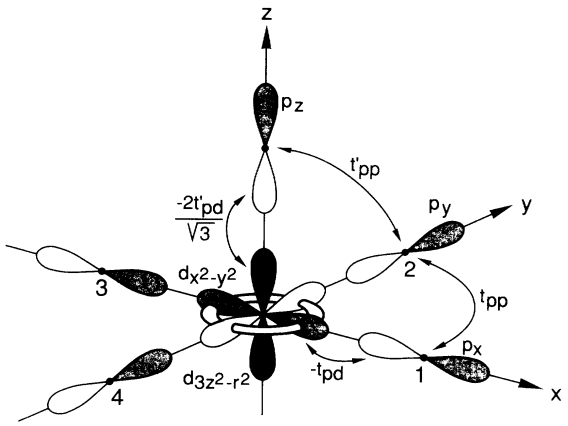

FIG. 1. Orbitals and phase convention (shaded lobes have positive sign) entering the five-band model; a unit cell contains the Cu ion, the planar-oxygen ions 1 and 2, and the apical oxygen(s).

stable and localized to give rise to a distinct singlet band within the charge-transfer gap. In this situation, the low-energy physics should be given by the (single-band) t-J model: positively charged holes (i.e., Zhang-Rice singlets) moving in a lattice of antiferromagnetically coupled spins. This would substantiate the original proposal by Anderson[11] that high-T_c superconductivity is to be found in the single-band Hubbard model, since the latter becomes equivalent to the t-J model in the strongly correlated limit.

However, it has also been argued that the spin of a hole on oxygen is a relevant independent degree of freedom[12] so that the oxygen band should be kept. In that case one would be left even in the strong-coupling limit with a two-band description: the Kondo-lattice model[13–19] where spin-carrying charged holes move on the oxygen lattice between the background of spins on the copper sites. Similarly, if the charge-transfer excitons are relevant, no reduction seems to be possible.

On the opposite side are proposals that the three-band model should be further augmented by additional orbitals. Calculations aiming at a realistic description of the electronic structure indicate[20–23] that more orbitals are involved in accommodating the holes than those considered so far, in particular at intermediate doping levels, and this is confirmed by various experiments. In particular, polarized x-ray-absorption spectroscopy[24,25] (XAS) and electron-energy-loss spectroscopy[26,27] (EELS) show a sizable ($\sim 10\%$) hole occupancy of the $d_{3z^2-r^2}$ (d_z) orbitals on copper. Also, XAS seems to indicate that the variation of that occupancy with doping and between the various cuprates correlates with the value of T_c, which suggests a role for the d_z orbital in bringing about high-T_c superconductivity, for example by the d-d excitation mechanism.[28,29] Including the copper d_z orbital results in a four-band model,[30] in which the planar-oxygen molecular orbital of local a_1 symmetry $\frac{1}{2}(p_{x_1}+p_{y_2}-p_{x_3}-p_{y_4})$ also gets mixed, viz., with the added d_z orbital. The feature of having two copper-centered orbitals of different symmetry leads to orbital-dependent superexchange (Kugel'-Khomskiĭ model[31,32]) and Jahn-Teller coupling to the lattice,[33] and upon doping to the possible formation of charged triplets in a background of spins (triplet t-J model[34]).

All these models are entirely restricted to the CuO_2 planes, and it would therefore only be possible to account for the differences between the various high-T_c compounds by using different in-plane parameters. In the actual cuprates, the copper ions are situated in pyramidal or octahedral structures and so they have apical oxygen ions above and/or below them. Several experimental findings indicate that these out-of-plane oxygen ions could be relevant to the superconductivity. For example, Raman spectroscopy[35] has shown a considerable softening below T_c of the mode involving the motion of the apical oxygen perpendicular to the CuO_2 plane. In this context it has been proposed that motion of the apical oxygen in a double-well potential, associated with strong charge transfer, is the source for superconductivity in the CuO_2 plane,[36] and quantum Monte Carlo simulations on simplified models[37,38] have demonstrated that such a mechanism is indeed viable. An analysis of the oxygen isotope effect[39] provides support for anharmonic motion of the apical oxygen linked to superconductivity, and direct evidence for the existence of a double-well potential in $YBa_2Cu_3O_7$ has recently been obtained from extended x-ray-absorption fine structure (EXAFS).[40]

Indications for the importance of the apical oxygens have also come from semiphenomenological analyses of the relation between crystal structure and the maximum critical temperature $T_c^{\max}$ in the various high-T_c cuprates. A clear correlation has been found between $T_c^{\max}$ and the Cu bond valence sum, which was shown to be almost entirely due to variation in bonding between the copper ion and the apical oxygen(s).[41] Similarly, a correlation has been demonstrated between $T_c^{\max}$ and the Madelung potential at the apical oxygen relative to the potential at the planar oxygens.[42] These findings suggest that *the apical oxygens affect the electronic structure in a way relevant to superconductivity*, despite the fact that their hole occupancy is small as has been shown by EELS.[26] However, this does not necessarily imply that the apical oxygens themselves are directly responsible for bringing about superconductivity. Actually, it would be quite compatible with the idea that the phenomenon of high-T_c superconductivity is strictly based on some peculiar properties of the electronic structure of the CuO_2 planes and might therefore be understood within one of the models mentioned above, but that those properties are affected by the apical oxygen ions. For example, it has been argued on the basis of cluster calculations that the correlation with the oxygen Madelung potential reflects a variation of the stability of the Zhang-Rice singlets.[43]

For the above reasons we investigate in the present work the effect of the apical oxygen(s) on the electronic structure of the CuO_2 plane. Our particular aim is to identify a characteristic feature in the electronic structure that is strongly affected by the apical oxygen(s) (and thus differentiates between the various cuprates), and which can also be shown to be related to high-T_c superconduc-

tivity. For that purpose we study a five-band model, which also includes, in addition to the most relevant planar orbitals (d_x, d_z, p_x, p_y), the p_z orbital on the apical oxygen, which can hybridize with the copper d_z orbital and with the planar-oxygen molecular orbital of local a_1 symmetry. We perform a band-structure analysis in the presence of strong correlations, which are handled by means of the slave boson technique in the mean-field approximation. In particular, we make a systematic investigation of the behavior of the occupancies of the various orbitals, both as a function of doping and as a function of the model parameters reflecting the differences between the various cuprates. We finally show that the total occupancy of all a_1 symmetry orbitals qualifies as the desired characteristic feature. The main result concerning the relation with high-T_c superconductivity is, as we have reported recently,[44] that for the hole-doped cuprates a correlation exists between the maximum critical temperature $T_c^{\max}$ attained in a particular compound and the quantity $n_{a_1}(\delta^{\max})-\delta^{\max}$, the excess density of holes in states with a_1 symmetry with respect to the doping $\delta^{\max}$ at which $T_c^{\max}$ is reached in that compound.

A similar attempt to correlate chemical structure, electronic structure, and the occurrence of high-T_c superconductivity has been made by Ohta *et al.*[43] They performed cluster calculations on Cu_2O_9 and Cu_2O_{11} clusters for virtually the same model as treated here, for an extensive collection of parameter sets representing all known cuprates containing CuO_2 planes. In the cluster approach, correlation effects and local hybridization are taken fully into account but the possible effect of band formation remains difficult to assess. In this respect the present approach offers a complementary view because band-formation effects are fully included but the correlations are treated in an approximate way. Moreover, the unavoidable limitation to clusters containing only two copper ions only allows calculations at effective doping levels of either 0 or 50 %, while the present approach allows a continuous variation of the doping level making it possible to investigate gradual changes with doping.

The plan of the paper is as follows. In Sec. II, we present the model, discuss the choice of parameters, and explain the treatment by the mean-field slave-boson method. The results of our systematic investigation of the electronic structure are presented in Sec. III: these concern the general features of the band structure and the Fermi surface, the orbital occupancies, the optical conductivity, and finally the occurrence of distortions. In Sec. IV, we compare these results with the data from various spectroscopies, and in Sec. V we discuss the connection between the occupancies and the semiempirical relation between crystal structure and critical temperature. Section VI is devoted to a discussion of the implications of our findings for various models and mechanisms for high-T_c superconductivity. Finally, we summarize our conclusions in Sec. VII.

II. FIVE-BAND EXTENDED HUBBARD MODEL

A. The electronic Hamiltonian

The Hamiltonian of the five-band model is

$$
\begin{aligned}
H=&\varepsilon_{d_x}\sum_{i,\sigma} d^{\dagger}_{xi,\sigma}d_{xi,\sigma}+\varepsilon_{d_z}\sum_{i,\sigma} d^{\dagger}_{zi,\sigma}d_{zi,\sigma}+\varepsilon_p\sum_{\substack{j,\sigma\\(\nu=x,y)}} p^{\dagger}_{\nu j,\sigma}p_{\nu j,\sigma}+\varepsilon_a\sum_{l,\sigma} p^{\dagger}_{al,\sigma}p_{al,\sigma}\\
&-2t_{pd}\sum_{k,\sigma}\{\sin(k_x/2)[(d^{\dagger}_x)_{k,\sigma}(p_x)_{k,\sigma}+\text{H.c.}]-\sin(k_y/2)[(d^{\dagger}_x)_{k,\sigma}(p_y)_{k,\sigma}+\text{H.c.}]\}\\
&+\frac{2t_{pd}}{\sqrt{3}}\sum_{k,\sigma}\{\sin(k_x/2)[(d^{\dagger}_z)_{k,\sigma}(p_x)_{k,\sigma}+\text{H.c.}]+\sin(k_y/2)[(d^{\dagger}_z)_{k,\sigma}(p_y)_{k,\sigma}+\text{H.c.}]\}\\
&+4t_{pp}\sum_{k,\sigma}\sin(k_x/2)\sin(k_y/2)[(p^{\dagger}_x)_{k,\sigma}(p_y)_{k,\sigma}+\text{H.c.}]-\frac{2t'_{pd}}{\sqrt{3}}\sum_{k,\sigma}[(d^{\dagger}_z)_{k,\sigma}(p_a)_{k,\sigma}+\text{H.c.}]\\
&+2t'_{pp}\sum_{k,\sigma}\{\sin(k_x/2)[(p^{\dagger}_x)_{k,\sigma}(p_a)_{k,\sigma}+\text{H.c.}]+\sin(k_y/2)[(p^{\dagger}_y)_{k,\sigma}(p_a)_{k,\sigma}+\text{H.c.}]\}\\
&+\frac{U_d}{2}\sum_{\substack{i,\sigma,\sigma'\\ \alpha,\beta=x,z}} d^{\dagger}_{\alpha i,\sigma}d_{\alpha i,\sigma}d^{\dagger}_{\beta i,\sigma'}d_{\beta i,\sigma'}(1-\delta_{\sigma\sigma'}\delta_{\alpha\beta})\\
&+\sum_{\substack{i,j,\sigma,\sigma'\\ \beta=x,z;(\nu=x,y)}} V_{\beta}d^{\dagger}_{\beta i,\sigma}d_{\beta i,\sigma}p^{\dagger}_{\nu j,\sigma'}p_{\nu j,\sigma'}+\sum_{\substack{i,l,\sigma,\sigma'\\ \beta=x,z}} V'_{\beta}\,d^{\dagger}_{\beta i,\sigma}d_{\beta i,\sigma}p^{\dagger}_{al,\sigma'}p_{al,\sigma'}\,,
\end{aligned}
\tag{1}
$$

where we work in the hole representation in which the vacuum state is the $3d^{10}$ configuration for copper and the $2p^6$ configuration for oxygen. The $d_{xi,\sigma}$ and $d_{zi,\sigma}$ ($d^{\dagger}_{xi,\sigma}$ and $d^{\dagger}_{zi,\sigma}$) operators are annihilation (creation) operators for holes in the $3d_{x^2-y^2}$ and $3d_{3z^2-r^2}$ orbitals of the Cu ions, $p_{xj,\sigma}$, $p_{yj,\sigma}$ ($p^{\dagger}_{xj,\sigma}$, $p^{\dagger}_{yj,\sigma}$) are the corresponding operators for the $2p_x$, $2p_y$ orbitals on the planar O sites while $p_{al,\sigma}$ ($p^{\dagger}_{al,\sigma}$) refer to the apical $2p_z$ O orbital.[45] The sub-

scripts i, j, and l indicate the Cu, planar O, and apical O sites, respectively (note that i and l refer to identical planar coordinates); the subscript k is used exclusively to indicate the (two-dimensional) wave vector; σ labels the spin. All summations over pairs of sites run over nearest neighbors only. The first four terms specify the *bare* atomic levels ε_p, ε_a, and $\varepsilon_{d_x}, \varepsilon_{d_z}$ for planar O, apical O, and Cu, respectively (allowing for a crystal-field splitting between the Cu $d_{x^2-y^2}$ and $d_{3z^2-r^2}$ orbitals). The following terms describe the various hybridizations, in accordance with the relative phases of the orbitals as shown in Fig. 1 and the associated sign convention for the hopping parameters,[46] but expressed in **k** representation (with the lattice constant a absorbed in the wave vector components k_x, k_y).[47] The fifth and sixth terms are the in-plane p-d hybridization, while the next term gives the dispersion of the planar-p band. The terms with the primed hopping parameters t'_{pd} and t'_{pp} describe the hybridization with the apical oxygen(s).[45] The U_d term is the strong Hubbard repulsion on Cu sites. We neglect the local and nearest-neighbor oxygen-oxygen repulsions.[48] The remaining terms give the nearest-neighbor Coulombic repulsions. Since the p_x and p_y orbitals overlap more with the $d_{x^2-y^2}$ orbitals than with the $d_{3z^2-r^2}$ ones, we assume $V_x > V_z$. For the same reason we consider two different values $V'_x < V'_z$ for the repulsions between holes in the p_a orbital and holes in the $d_{x^2-y^2}$ or $d_{3z^2-r^2}$ orbitals, respectively.

The strong Hubbard U_d repulsion forbids double hole occupancy on the copper. This has been formalized by means of the slave-boson approach,[49] which, in the limit $U_d \to \infty$, leads to $b_i^\dagger b_i + n_{d_{xi}} + n_{d_{zi}} = 1$, where $b_i^\dagger$ and b_i are the slave-boson operators of the standard replacement of the d and $d^\dagger$ operators $d^\dagger \to d^\dagger b$, $d \to b^\dagger d$. The constraint is then implemented by a Lagrange multiplier field λ_i. The V terms are decoupled via Hubbard-Stratonovich transformations which introduce eight complex pairwise conjugate auxiliary fields. At the mean-field level we set all these fields, including b_i and λ_i, equal to their average values independent of the site. To get these (not all independent) mean-field parameters, we solve numerically the self-consistency equations together with the equation for the chemical potential which fixes the average number of particles per cell to the value $n = 1 + \delta$, where δ is the doping. Once the mean-field parameters are obtained, they can be inserted into the Hamiltonian and its diagonalization gives the band structure. In the Appendix we give a more detailed description of this procedure.

The model parameters for our calculations were chosen as follows. When we investigate the influence of the apical oxygens on the electronic structure in general (Sec. III), we make a systematic variation of the parameters ε_a and t'_{pd} (and t'_{pp}) which control the interaction between the apical oxygens and the CuO_2 plane (in short, the apex-plane interaction), while keeping the parameters referring to the CuO_2 plane fixed. For these in-plane parameters we have considered two distinct parameter sets. They correspond to the two different regimes that exist in the model because of the Brinkman-Rice-like metal-insulator transition at zero doping that was already found in the slave-boson mean-field (SBMF) treatment of the three-band model:[50,51] if the bare charge-transfer energy $\Delta = \varepsilon_p - \varepsilon_{d_x}$ is below a critical value Δ_c, the model shows metallic behavior in the limit of vanishing doping in the sense that b^2 remains finite so that the bands remain dispersive (although with high mass) and the Fermi surface persists, while the system is insulating in the sense that b^2 goes to zero if Δ is larger than Δ_c.

In both parameter sets the in-plane hopping parameters t_{pd} and t_{pp} have been taken in accordance with the estimates for the high-T_c cuprates from photoelectron spectroscopy[52] and (constrained) local-density-approximation (LDA) calculations.[53,54] In our first parameter set (given in Table I, labeled "metallic"), the value of the bare charge-transfer energy is smaller than Δ_c, while the value in the second set (labeled "insulating") is larger than Δ_c. Actually, the smaller value (3 eV) is the one obtained from the mentioned estimates for the cuprates, and although this value reproduces the experimentally observed charge-transfer gap in fully correlated cluster model calculations,[9] it corresponds, in fact, to the metallic regime in the present approach. For the high-T_c cuprates, which are actually insulators at low doping, this might be considered essentially an artifact of the present SBMF approximation, which overestimates Δ_c because it does not allow for local (intracell) hybridization without the occurrence of full band formation and therefore produces metallic behavior too readily (i.e., even for large Δ) in order to make the system gain kinetic energy from the hopping matrix elements. Since it is not quite obvious whether the physics of the cuprates is better represented by keeping the original parameters (and discarding the results at low doping) or by modifying them such as to force the model to show the desired insulating behavior at low doping, we wanted the value for Δ in the second parameter set to be $> \Delta_c$ but still quite close to the estimated value for the cuprates, and have set it arbitrarily at 5 eV. For the nearest neighbor Coulomb repulsions an upper limit of 1 eV has been estimated from Auger spectroscopy.[55] We have therefore taken as typical values $V_x = 0.5$ eV, $V_z = 0.25$ eV, $V'_x = 0.1$ eV, and $V'_z = 0.5$ eV.

As regards the parameters characterizing the apical oxygen, we made sure that their variation covered the range from where the p_a orbital is strongly coupled to the orbitals in the CuO_2 plane to where it has become virtually ineffective and the model reduces to the four-band

TABLE I. Standard set of in-plane model parameters, all energies in eV.

$t_{pd} = 1.0$	$V_x = 0.5$
$t_{pp} = 0.4$	$V_z = 0.25$
$\varepsilon_{d_x} = 0.0$	$V'_x = 0.1$
$\varepsilon_{d_z} = 0.3$	$V'_z = 0.5$
ε_p (metallic) $= 3.0$	
ε_p (insulating) $= 5.0$	

model. Because the energy level of p_a is determined by the Madelung potential at the apical oxygen site, while the hopping matrix elements t'_{pd} and t'_{pp} are determined by the distance of the apical oxygen from the CuO_2 plane, we varied ε_a and t'_{pd} independently, but made t'_{pp} track t'_{pd}. We assumed the usual r^{-3} and r^{-4} distance dependence for p-p and p-d tight-binding parameters[56] taking also the varying angle between apical and planar-oxygen p orbital into account, and chose the proportionality constants such that the apical oxygen hopping parameters are equal to those in the plane when the apex-copper distance equals the planar oxygen-copper distance. The nearest-neighbor Coulomb integrals involving the apical oxygen were set to fixed values consistent with those in the plane and corresponding to an about 25% larger apex-copper distance. No variation with distance was implemented because it almost did not affect the results.

When we perform calculations for specific compounds (Sec. V) in order to correlate the results with the observed critical temperatures, we follow the procedure of Ref. 43 and determine the parameters according to the structural data in that paper. Thus, the hopping matrix elements are based upon the estimated values for t_{pd} and t_{pp} for La_2CuO_4, with the variation in apex-copper and planar oxygen-copper distance in the various compounds being accounted for by the procedure indicated above. The bare atomic levels are derived from the Madelung potentials calculated in the ionic model and reduced by the optical dielectric constant, taken equal to 3.5, and from the difference between the second ionization potential of copper and the second electron affinity of oxygen, taken equal to 12 eV. For the copper-oxygen Coulomb repulsion parameters, we use throughout the same values as above.

B. Electron-phonon interaction

We shall also investigate whether in some circumstances the electronic structure can give rise to a lattice instability, and, in particular, if a Peierls transition could occur. We therefore need to know how the electronic structure is affected by lattice deformation. Within the present tight-binding description this comes about because the hopping matrix elements are (rather strongly) dependent on the interatomic distance, and displacements of ions will thus give rise to changes in hybridization. We may therefore derive the electron-phonon interaction by expanding the hopping terms in (1) with respect to displacements of the ions from their assumed equilibrium positions in the square lattice and expressing the displacements in term of strain and phonon coordinates. Since the hybridization is for the most part in the CuO_2 plane, we consider here only in-plane motion of the Cu and planar-O ions, and further restrict ourselves to the phonon part. We then obtain the following electron-phonon interaction Hamiltonian:

$$
\begin{aligned}
H_{\text{el-ph}} = & -g_p \sum_{q,s} u_q^{(s)} \sum_{k,\sigma} \zeta_s(k,q)[(p_y^\dagger)_{k+q,\sigma}(p_x)_{k,\sigma} + \text{H.c.}] \\
& + g \sum_{q,s} \eta_s^x(q) u_q^{(s)} \sum_{k,\sigma} \sin(k_x/2)[(d_x^\dagger)_{k+q,\sigma}(p_x)_{k,\sigma} + \text{H.c.}] \\
& - g \sum_{q,s} \eta_s^y(q) u_q^{(s)} \sum_{k,\sigma} \sin(k_y/2)[(d_x^\dagger)_{k+q,\sigma}(p_y)_{k,\sigma} + \text{H.c.}] \\
& - \frac{g}{\sqrt{3}} \sum_{q,s} \eta_s^x(q) u_q^{(s)} \sum_{k,\sigma} \sin(k_x/2)[(d_z^\dagger)_{k+q,\sigma}(p_x)_{k,\sigma} + \text{H.c.}] \\
& - \frac{g}{\sqrt{3}} \sum_{q,s} \eta_s^y(q) u_q^{(s)} \sum_{k,\sigma} \sin(k_y/2)[(d_z^\dagger)_{k+q,\sigma}(p_y)_{k,\sigma} + \text{H.c.}] ,
\end{aligned} \tag{2}
$$

where $u_q^{(s)}$ is the amplitude of the lattice mode from branch s with wave vector q, and the coupling constants are given by $g = -dt_{pd}(r)/dr|_{r=a/2}$ and $g_p = -dt_{pp}(r)/dr|_{r=a/\sqrt{2}}$, where a is the lattice constant. Further,

$$
\eta_s^x(q) = \frac{2i}{\sqrt{N_c m_O}} \sin(q_x/2) e_q(x1|s) , \tag{3}
$$

$$
\eta_s^y(q) = \frac{2i}{\sqrt{N_c m_O}} \sin(q_y/2) e_q(y2|s) , \tag{4}
$$

and

$$
\begin{aligned}
\zeta_s(k,q) = & \frac{2\sqrt{2}i}{\sqrt{N_c m_O}} \{ \cos(k_x/2)\sin(k_y/2) e_q(x2|s) + \sin(k_x/2)\cos(k_y/2) e_q(y2|s) \\
& - \cos[(k_x+q_x)/2]\sin[(k_y+q_y)/2] e_q(x1|s) \\
& - \sin[(k_x+q_x)/2]\cos[(k_y+q_y)/2] e_q(y1|s) \} ,
\end{aligned} \tag{5}
$$

where $e_q(x1|s)$ is the component of the phonon polarization vector of the lattice mode along the x displacement of oxygen ion 1 (carrying the p_x orbital, see Fig. 1), etc., N_c is the number of unit cells, and m_O is the mass of the oxygen ion. We must also include an elastic energy contribution from the lattice

$$H_{\text{latt}}=\tfrac{1}{2}\sum_{q,s}[\omega_q^{(s)}]^2 u_q^{(s)} u_{-q}^{(s)} , \tag{6}$$

which supplies stability, and may be thought of as arising from the repulsion between the ion cores.

We note that the electron-phonon interaction involves only displacements of oxygen ions; the changes in hybridization caused by the displacement of a copper ion cancel in lowest order. Therefore, only a single atomic mass appears in Eqs. (3)–(5) and one can conveniently define for the relevant modes $\bar{u}_q^{(s)}=u_q^{(s)}/(\sqrt{N_c m_O}a/2)$. This dimensionless phonon coordinate, when multiplied by the appropriate component of the phonon polarization vector, then gives the relative displacement of an oxygen ion in the mode (apart from a phase factor related to the position of the oxygen in the unit cell). After corresponding redefinition of $\bar{\eta}_s^{\alpha}(q)=\sqrt{N_c m_O}\eta_s^{\alpha}(q)$ and $\bar{\xi}_s(k,q)=\sqrt{N_c m_O}\xi_s(k,q)/\sqrt{2}$, and of the coupling constants $\bar{g}=-r\,dt_{pd}(r)/dr|_{a/2}$ and $\bar{g}_p=-r\,dt_{pp}(r)/dr|_{a/\sqrt{2}}$, the electron-phonon interaction retains the same form when reexpressed in the "barred" quantities. The contribution to the lattice energy from the mode in branch s with wave vector q can be rewritten as $\frac{1}{2}N_c E_{q,s}\bar{u}_q^{(s)}\bar{u}_{-q}^{(s)}$, where $E_{q,s}=m_O[\omega_q^{(s)}]^2(a/2)^2$.

We investigate the effect of deformations by the frozen-phonon approach: the electronic structure and, in particular, the energy of the system is calculated for a fixed deformation in a particular lattice mode, and the phonon amplitude is thus treated as a classical variable. The additional contribution to the mean-field Hamiltonian from the electron-phonon interaction is then obtained from Eq. (2) by inserting a boson expectation value b in the terms involving a d orbital. Since its derivative with respect to b is therefore nonzero, it also generates an extra term in the corresponding self-consistency equation (see the Appendix).

We now must find out which lattice modes involve oxygen displacements that produce the strongest coupling to the electrons. Of particular importance are zone-boundary modes which could induce a structural phase transition of the simplest type, i.e., by cell doubling. In order to identify these modes and to estimate the frequencies $\omega_q^{(s)}$, we adopt a simple but explicit model. It contains two force constants to describe the forces between the ions in the CuO_2 plane, a Cu-O stretch C, and an O-O stretch C_O.[57] It is then straightforward to write down the dynamical matrix for the six phonon branches associated with the motion of the ions in the CuO_2 plane, and derive expressions for the frequencies of particular modes at special points in the Brillouin zone (and find their polarization vectors), and for the sound velocities. Of most interest are the modes involving stretching of the Cu-O bond because they give the strongest electron-phonon interaction [see Eqs. (3) and (4)] and also because they are most easily identified in the experimental spectra. We thus identify an M point [$\equiv(\pi/a,\pi/a)$] breathing mode [all four planar oxygens moving alternatingly inward on or outward from the Cu ion, $e_M(x1|b)=e_M(y2|b)=-i/\sqrt{2}$, all other components $e_M(\cdots|b)=0$] and an M-point quadrupolar mode [two oxygens moving inward, two outward, $e_M(x1|q)=-e_M(y2|q)=-i/\sqrt{2}$] with frequencies $\omega_M^{(b)}=\sqrt{(4C_O+2C)/m_O}$ and $\omega_M^{(q)}=\sqrt{2C/m_O}$, respectively. We further obtain at the X point [$\equiv(\pi/a,0)$] a semiquadrupolar mode [the oxygen ions along the x axis moving alternatingly to the right and to the left, $e_X(x1|sq)=-i$, so that the Cu ions have alternatingly two inmoving or outmoving oxygen neighbors] with frequency $\omega_X^{(sq)}=\sqrt{(2C_O+2C)/m_O}$. The velocities of [longitudinal (L) and transverse (T)] acoustic waves with wave vector along ΓX are $v_L^{\Gamma X}=\sqrt{(C+C_O)/2\rho}$ and $v_T^{\Gamma X}=\sqrt{C_O/2\rho}$, and those with wave vector along ΓM are $v_L^{\Gamma M}=\sqrt{(C/4+C_O)/\rho}$ and $v_T^{\Gamma M}=\sqrt{C/4\rho}$, where ρ is the mass per unit area, $\rho=(M+2m_O)/a^2$, with M being the mass of the Cu ion.

In order to estimate the frequencies to be used in the actual calculations, we proceed as follows. We first apply our lattice model to the actual phonon dispersion curves as determined by inelastic neutron scattering, and use it to derive the frequencies of interest from the features identified with greatest certainty. So we observe[58] that, in La_2CuO_4, the frequency of the M-point quadrupolar mode is about 15 THz ($\equiv$62 meV), yielding $C\approx 1.2\times 10^5$ dyn/cm. From the fact that the ratio between the longitudinal and the transverse sound velocity along ΓX is ≈ 2, one finds that $C\approx 3C_O$, leading to $C_O\approx 0.40\times 10^5$ dyn/cm. This would put the other frequencies at $\hbar\omega_M^{(b)}\approx 80$ meV ($\equiv$19 THz) and $\hbar\omega_X^{(sq)}\approx 72$ meV ($\equiv$17 THz). In $YBa_2Cu_3O_7$, the frequency of the M-point breathing mode corresponds to[59] $\hbar\omega_M^{(b)}\approx 75$ meV ($\equiv$18 THz) leading to very similar values. These actual frequencies, of course, include the response of the electrons, i.e, they are already "renormalized" by the electron-phonon interaction. Therefore, we next perform small-amplitude frozen-phonon calculations for the mode of interest with a doping value for which no instability is expected and determine the "bare" frequency that produces the desired renormalized frequency when both the bare elastic energy and the change in the energy of the electron system upon deformation are included. This bare frequency is then used for the actual calculation in the doping regime where an instability could occur.

If the p-d and p-p hopping matrix elements are assumed to depend on distance like $1/r^{\alpha_{pd}}$ and $1/r^{\alpha_{pp}}$, respectively, the coupling constants are simply related to the hopping matrix elements at equilibrium distance by $\bar{g}=\alpha_{pd}t_{pd}$ and $\bar{g}_p=\alpha_{pp}t_{pp}$. Consistent with our treatment of the apex-plane hopping parameters, we have therefore, in general, taken $\bar{g}=4t_{pd}$ and $\bar{g}_p=3t_{pp}$, but we have also briefly investigated the effect of a stronger electron-phonon coupling equivalent to a larger value of α_{pd}.

III. RESULTS: ELECTRONIC STRUCTURE

A. Band structure and Fermi surface

We first consider qualitative aspects of our results, like the general appearance of the band structure and the

shape of the Fermi surface, which are illustrated in Fig. 2 (for $\Delta=3$ eV, i.e., in the "metallic" regime).

The most important feature is that there are always two quasiparticle bands in the vicinity of the Fermi level. They originate from the renormalized Cu d_x and d_z levels, which have acquired dispersion from the hybridization with the in-plane oxygen orbitals, and have (anti-) crossed halfway the Brillouin zone. Consequently, the composition of these bands is rather complicated: both have components along all five states but the amplitudes vary considerably with k. The lowest band is of predominantly d_x character in the outer part of the Brillouin zone, but predominantly d_z near the Γ point, while the situation is reversed for the second band. However, the amount of planar-oxygen orbitals mixed in is substantial, in particular at higher doping levels, so that it is more accurate to say that the local symmetry of the lower (second) band is largely b_1 (a_1) in the outer part of the Brillouin zone (BZ) and largely a_1 (b_1) near the center, as can be verified by projection.

A relevant role in this electronic structure is played by the p_a orbitals of the apical oxygen ions because the p_a orbitals can hybridize with the d_z orbitals of the copper ions and the a_1 symmetry combination of p_x and p_y orbitals of the oxygen ions in the plane. As it turns out, this hybridization is rather effective and it lowers the energy of the second (predominantly a_1) band, enhances the mixing of the two bands, and increases the a_1 contribution to the states occupied by holes. It must be emphasized, however, that the main effect of the apical oxygens is indirect: the p_a orbitals modify the occupation of planar orbitals of a_1 symmetry, while keeping their own occupancy rather small.

The b_1 branch is essentially the band obtained by Kotliar, Lee, and Read[50] in their mean-field slave-boson treatment of the three-band model. It can be considered as the representation of the Zhang-Rice singlet band since the Zhang-Rice singlet is built in the localized picture from molecular orbitals of b_1 symmetry only. The identification is, however, not complete, not only because

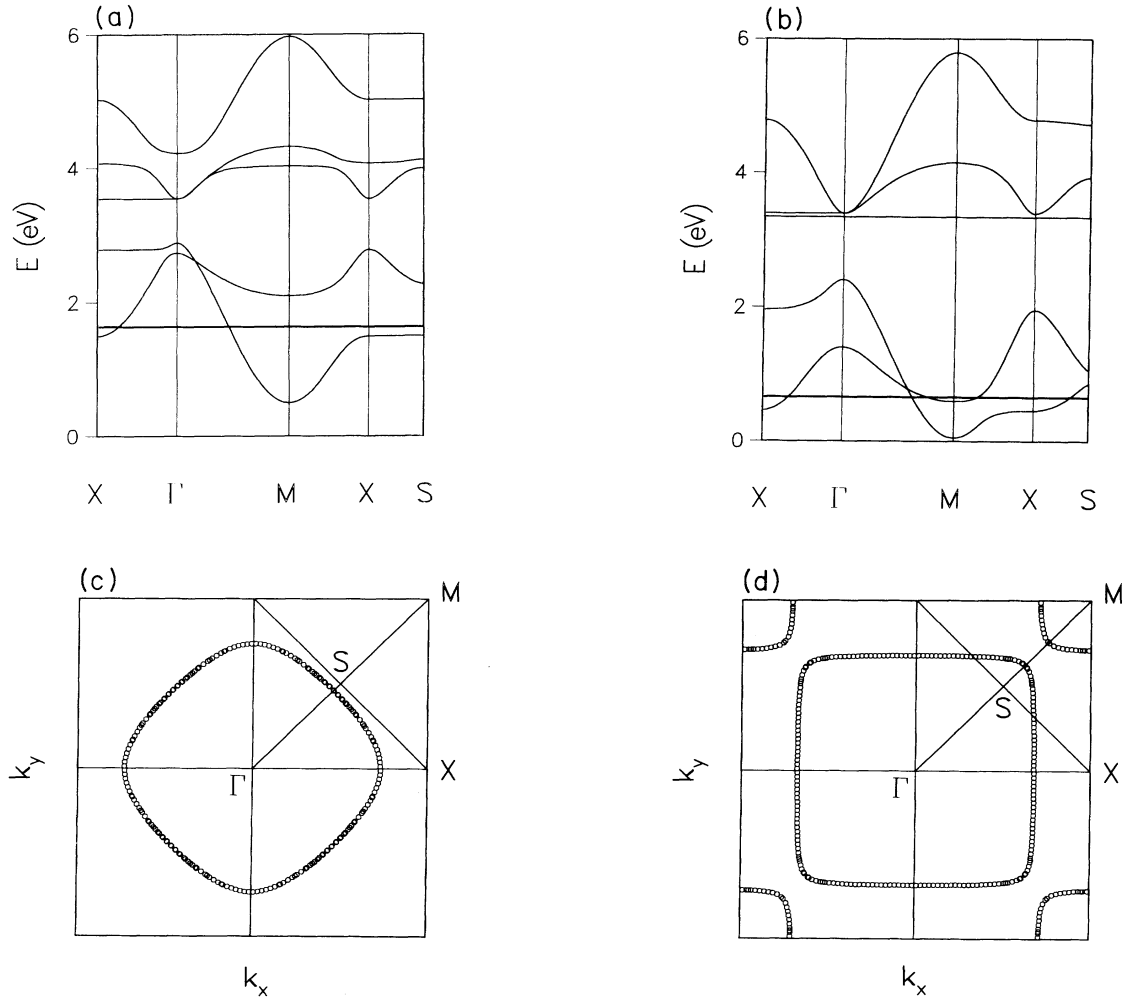

FIG. 2. (a) and (b) Band structure and (c) and (d) Fermi surface in the metallic regime ($\Delta=3$) for (a) and (c) weak apex-plane coupling, $\varepsilon_a=4$, $t'_{pd}=0.4$, $t'_{pp}=0.267$, and (b) and (d) strong apex-plane coupling, $\varepsilon_a=2$, $t'_{pd}=0.8$, $t'_{pp}=0.367$; for both cases doping $\delta=0.25$, and all other parameters as in Table I (all the energies are in eV); in (a) and (b) the Fermi level is indicated by the thick horizontal line.

the singlet character itself is, of course, absent in the present spin-independent treatment, but also because of the mixed character of the two bands: e.g., there is a nonzero d_z component (of a_1 symmetry) even in the b_1-dominated part of the lowest band.

The a_1 branch represents an additional degree of freedom. Obviously it is associated with the near degeneracy of the Cu (d_x and d_z) orbitals. It can also be considered to reflect the presence of an oxygen $p\sigma$ band in the CuO_2 plane that is independent of the copper spins already present in the undoped plane.[12]

It further turns out that two quite distinct situations may occur, of which Fig. 2 shows typical examples. The first situation is where only the lowest band crosses the Fermi level (one-band situation: 1 BS). This is realized for moderate doping if the apex-plane interaction is not too strong, and the resulting band structure and Fermi surface are shown in Figs. 2(a) and 2(c). It follows from the previous discussion that the local orbitals occupied by holes are largely of b_1 symmetry. The Fermi surface is rather smooth in this case, with a tendency towards the development of flat portions parallel to the diagonals. The holes occupy the outer part of the Brillouin zone, and the Fermi surface should be called electronlike.

The second situation is where the second band also crosses the Fermi level (two-band situation: 2BS). This is shown in Figs. 2(b) and 2(d), and occurs for high doping or for strong apex-plane interaction (i.e., small $\varepsilon_a-\varepsilon_p$ and/or large t'_{pd} and t'_{pp}). Now a larger fraction of the holes occupies orbitals of local a_1 symmetry, in fact not only because the occupied part of the second band has largely a_1 character but also because the occupied part of the lowest band has more a_1 mixed in under the circumstances where the second band is able to cross. However, since the lowest band still contains the majority of the holes (more than 1 per unit cell) and the lower part of it is still largely b_1-like, the b_1 occupancy, in general, still exceeds the a_1 occupancy. In this 2BS, the Fermi surface has, of course, two separate parts. The second band gives rise to hole pockets in the corners of the Brillouin zone, while the part of the Fermi surface associated with the lowest band is now almost square and has changed its orientation, the sides being parallel to the k_x,k_y axes instead of to the diagonals. One would expect that the flat portions of the Fermi surface associated with the lowest band could give rise to macroscopic distortions, and the possibility that a Peierls instability might occur will be discussed in Sec. III D.

Next, let us consider in some more detail the conditions that determine whether the one-band or the two-band situation actually occurs. As mentioned above, for not too low ε_a and not too large t'_{pd} (and t'_{pp}), the 1BS will be realized at low doping, with the bottom of the second (a_1-like) band, which is at the M point [$\equiv(\pi/a,\pi/a)$], lying a finite distance above the Fermi level. If δ increases (at fixed structural parameters) that distance decreases, simply because the Fermi level moves upwards while the positions of the bands remain virtually unchanged. At a critical doping level δ_c (the value of which depends on the structural parameters), the Fermi level reaches the bottom of the second band, and upon a further increase of the doping one enters the 2BS regime.

The influence of the apical oxygen is most readily seen from the dependence of δ_c on ε_a and t'_{pd}, which is shown in Fig. 3. It is obvious that a stronger involvement of the apical ion, either because of a larger hopping integral between apical ion and CuO_2 plane or because of a lower position of the energy level of the apical orbital, favors the two-band situation. For ε_a well below ε_p and t'_{pd} of the order of or larger than t_{pd}, one finds that $\delta_c=0$, so that actually the 2BS occurs for any finite δ. This behavior is readily understood from the local picture: the apical p_a orbital, by hybridizing with the other a_1 states (d_z and p_{a_1}) lowers the lowest a_1 state with respect to the b_1 states, and therefore pushes down the mainly a_1-like bottom of the second band with respect to the predominantly b_1-like lowest band. (This also makes it understandable that the effect of the apical orbital can be mimicked to some extent within the four-band model, where p_a itself is omitted, by reversing the sign of t_{pp}: this inverts the order of the two planar-oxygen p bands, putting the a_1 band below the b_1 band.[30]) It should be pointed out that, if the apical ion is virtually decoupled from the CuO_2 plane ($\varepsilon_a\gg\varepsilon_p$ and/or $t'_{pd}=0$), δ_c is so large (≥ 0.5) that for any value of doping that is realistic for the high-T_c cuprates one will always find the 1BS. So within the present model, the apical oxygen ion appears to be essential for having two, instead of one, quasiparticle bands being partially occupied.

Finally, we comment briefly on the effect of the structural parameters related to the orbitals in the CuO_2 plane. For $\Delta=5$ eV, i.e., in the "insulating" regime, we find the overall form of the band structure and the Fermi surface to be very similar to that described above, and we also obtain the same transition behavior between the 1BS and 2BS, the dependence of δ_c on t'_{pd} and $\varepsilon_a-\varepsilon_p$ being also almost identical. There is, however, one major difference with the "metallic" regime: the bands lie closer to each other and are narrower by about a factor 2,

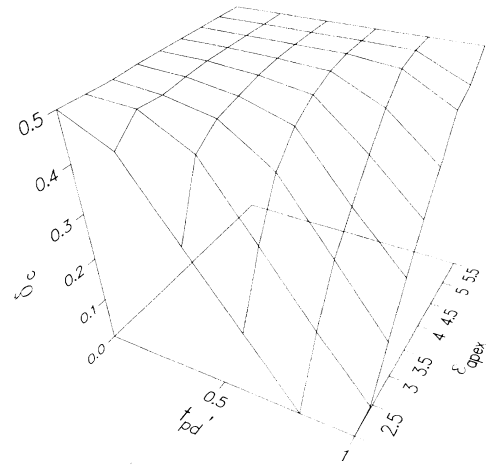

FIG. 3. Critical doping vs apical oxygen orbital energy and apex-plane hopping matrix element in the metallic regime, i.e, $\Delta=3$ eV and all other parameter as in Table I; the flat part at the upper left represents the region where δ_c is larger than 0.5.

reflecting the more insulating behavior brought about by the smaller value of b and the resulting weaker hybridization.

B. Orbital occupancies

We now turn our attention to the densities of holes in the various orbitals. In addition to the occupation of the five orbitals individually, we shall also consider the densities classified according to the local symmetry of the orbitals. These are n_{a_1}, the total occupancy of all states with local a_1 symmetry (i.e., resulting from d_x, from the apical oxygen p_a orbital, and from the a_1-symmetric combination of the planar-oxygen orbitals), and n_{b_1}, the occupancy of the states with local b_1 symmetry (i.e., from d_x and from the b_1-symmetric combination of the planar-oxygen orbitals). The contributions from the planar oxygens are obtained by projecting the occupied states on

$$(p_{a_1})_{k,\sigma}=[\sin(k_x/2)(p_x)_{k,\sigma}+\sin(k_y/2)(p_y)_{k,\sigma}]/\gamma_k \quad (7)$$

and

$$(p_{b_1})_{k,\sigma}=[\sin(k_x/2)(p_x)_{k,\sigma}-\sin(k_y/2)(p_y)_{k,\sigma}]/\gamma_k \ , \quad (8)$$

where $\gamma_k^2 \equiv \sin^2(k_x/2)+\sin^2(k_y/2)$. One should note that, since these states are, in general, not orthogonal, n_{a_1} and n_{b_1} are not just complementary quantities, i.e, $n_{a_1}+n_{b_1}=1+\delta$ holds only approximately, although the deviation is usually smaller than 10%.

It is important to distinguish between changes in the occupancies upon variation of doping for fixed model parameters (i.e., in a particular compound) and upon variation of model parameters (i.e., of crystal structure between different compounds) at a fixed value of the doping. We consider first the dependence on doping, which is shown in Fig. 4 for two characteristic parameter sets, both in the "metallic" regime: in Figs. 4(a) and 4(c) for t'_{pd} small and ε_a well above ε_p so that the influence of the apical oxygen is small, in Figs. 4(b) and 4(d) for a fairly strong apex-plane interaction. The overall behavior is seen to be rather similar in the two cases. For all occupancies the change with doping is approximately linear, i.e., the "added" holes distribute themselves in a nearly doping-independent ratio over the orbitals. As regards the individual orbitals, the largest increase with increasing δ occurs in n_p, the occupancy of the planar-oxygen orbitals, reflecting the well-known fact that the doped holes go largely on oxygen sites because of the strong Coulomb repulsion on the copper ions. There is a finite occupancy n_z of the d_z orbitals which grows gradually but distinctly with doping, while the d_x occupancy n_x decreases very slightly. Also, the occupancy of the apical oxygen orbital n_a increases with δ, in particular for the

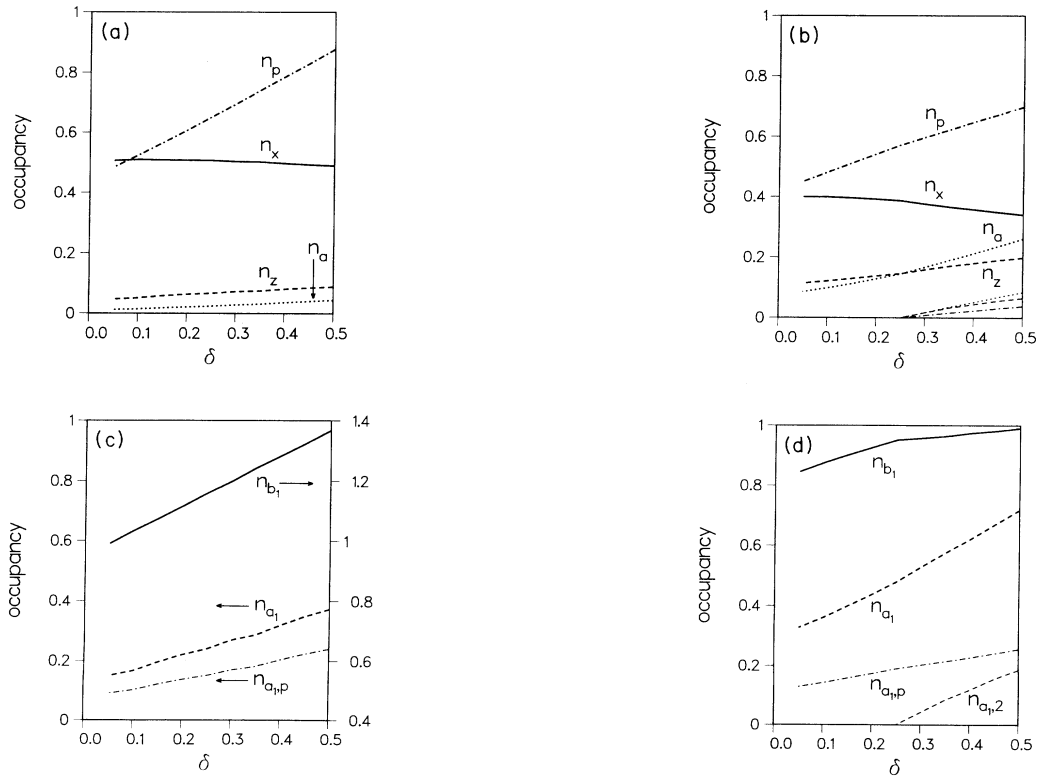

FIG. 4. Orbital occupancies as a function of doping in the metallic regime ($\Delta=3$) for (a) and (c) weak apex-plane coupling, and (b) and (d) strong apex-plane coupling (all model parameters as in Fig. 2); thick lines: total occupancies (i.e., from all bands); thin lines in (b) and (d): contributions from second band; thin dashed-dotted line in (c) and (d): contribution to n_{a_1} from planar-oxygen orbitals.

stronger apex-plane interaction. As regards the symmetry of the occupied states, Figs. 4(c) and 4(d) show that both n_{b_1} and n_{a_1} increases with doping, but n_{a_1} increases relatively more, in particular for stronger apex-plane interaction. This is not only due to the relatively large increase in n_z and n_a, but also to the overlap of the (large and increasing) planar-oxygen component of the occupied states with the a_1-symmetry orbitals [Eq. (7)] (this contribution is shown by the dash-dotted line).

While the variation with δ is similar in Figs. 4(a) and 4(c) as compared to Figs. 4(b) and 4(d), the magnitudes of the occupancies are considerably different. In particular, both n_z and n_a are seen to be much larger when the apex-plane interaction is strong, which is compensated by smaller values of n_x and n_p. As far as the copper orbitals are concerned, it is not the slopes of the curves that are different but rather the limiting values at low doping: the "preexistent" holes are distributed differently between d_x and d_z. As regards the oxygen orbitals, n_a also grows more rapidly with doping and n_p slower for stronger apex-plane interaction: also the "added" holes go to a lesser extent onto the planar oxygens and rather more on the apicals.

The dependence on the input parameters referring to the apical oxygen, t'_{pd} and ε_a, is shown in greater detail in Figs. 5 and 6, respectively, each for two different values of the doping. One observes that the interaction between the CuO_2 plane and the apical oxygen enhances the occupation of the d_z orbital and that of the apical oxygen p_a orbital, while that of the d_x orbital and that of the planar-oxygen orbitals are accordingly reduced. An increase of t'_{pd}, corresponding to a decrease in the distance between apical oxygen and copper ions, affects n_z and n_a about equally, and n_x more than n_p. As one would expect, a decrease of ε_a, corresponding to a lowering of the Madelung potential at the apical oxygen site, has a larger effect on the occupancy of the apical oxygen orbital itself than on n_z, and affects n_p more than n_x, in particular when ε_a falls below ε_p. As Figs. 5(c) and 5(d) and 6(c) and 6(d) show, these changes are reflected in an increase of n_{a_1} at the expense of n_{b_1} with increasing apex-plane interaction. This is not only due to the increasing occupancy of the d_z and apical p_a orbitals but also to the increase of the a_1-symmetry content in the planar-oxygen component, although n_p decreases. It is also seen that the a_1 enhancement becomes slightly stronger for larger doping: this is easily understood if one realizes that the upper part of the lowest band and the lower part of the second band, being both a_1-like, are affected most by mixing with the p_a orbital.

We should further point out that the increase in n_{a_1} is not directly related to the occupation of states in the second band. The increase already occurs well before the apex-plane interaction is strong enough to make the second band cross the Fermi level. Returning to Figs. 4(b) and 4(d), one observes only a slight kink in the total occupancies when the crossing actually takes place, revealing the somewhat different composition of the states in the second band. For illustration, the contributions from the second band are shown separately: although these are indeed purely a_1-like, the largest contribution

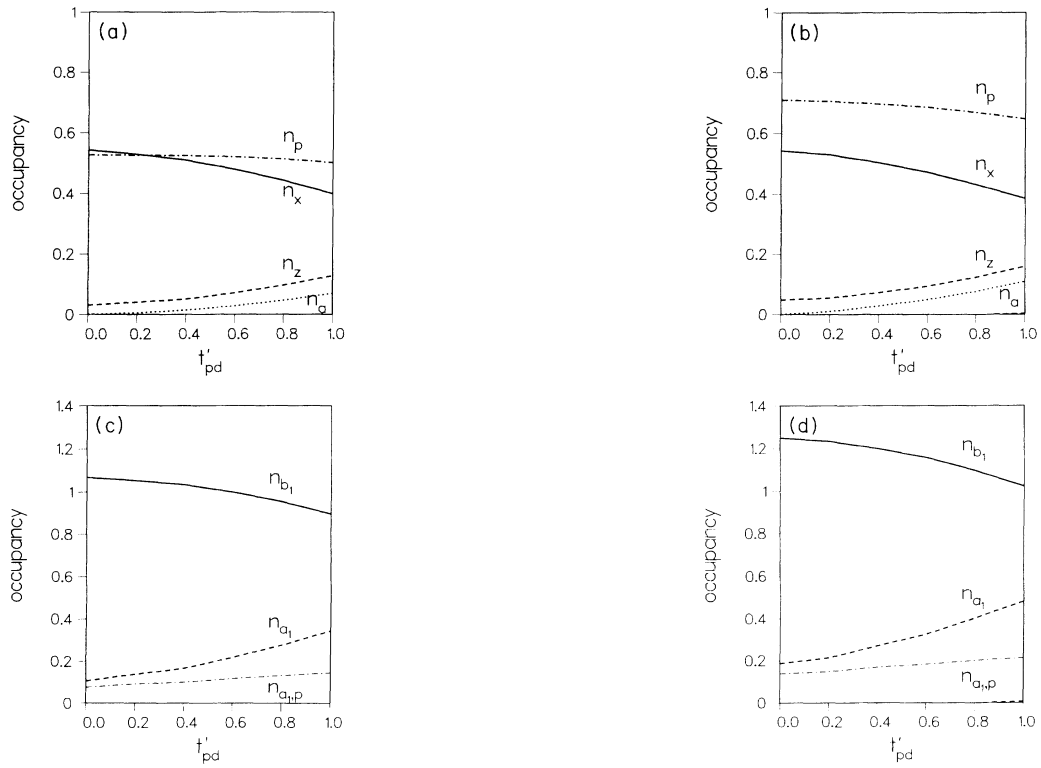

FIG. 5: Orbital occupancies vs apex-plane hopping matrix element in the metallic regime ($\Delta=3$) for $\varepsilon_a=4$: (a) and (c) $\delta=0.1$, (b) and (d) $\delta=0.3$; all other parameters as in Table I; meaning of lines as in Fig. 4.

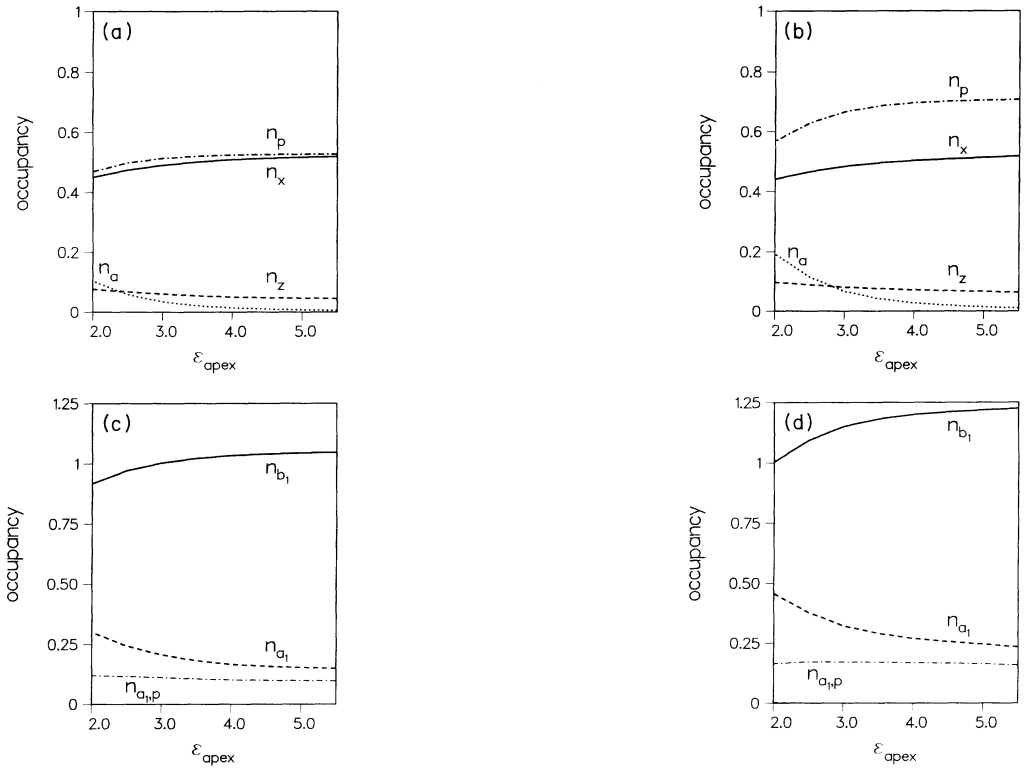

FIG. 6. Orbital occupancies vs apical oxygen orbital energy ($\varepsilon_{apex} \equiv \varepsilon_a$) in the metallic regime ($\Delta = 3$) for $t'_{pd} = 0.4$, $t'_{pp} = 0.267$: (a) and (c) $\delta = 0.1$, (b) and (d) $\delta = 0.3$; all other parameters as in Table I; meaning of lines as in Fig. 4.

to n_{a_1} still comes from the lowest band. The situation is best summarized by saying that the coupling of the CuO_2 plane to the apical oxygen first leads to an increase of the occupancy of states of a_1 symmetry by modifying the character of the lowest band,and only when sufficiently strong can lead in addition to the crossing of the Fermi level by the second band giving rise to a further enhancement of n_{a_1}.

We now recognize an important distinction between the effect of increasing doping and increasing apex-plane interaction, although both lead to a relative enhancement of local a_1 symmetry of holes. In the case of doping this occurs because the added holes have to go into the higher-lying states which are more a_1-like than those occupied by the holes already present. In contrast, the apex-plane interaction makes both the added and the preexistent holes more a_1-like because it enhances the a_1 character of all relevant states.

Finally, we look again briefly at the behavior in the "insulating" regime, illustrated in Figs. 7–9. The differences with the metallic regime arise from the smaller hybridization, which makes the b_1-like band more predominantly d_x and the a_1-like band predominantly d_z, and also reduces the overall mixing of the two bands. This results in much larger values for n_x and correspondingly smaller n_p, while n_z is about the same because opposing effects cancel, and n_a is slightly reduced. As Fig. 7 shows, in addition the dependence of the occupancies on doping is now distinctly nonlinear, in particular for n_x and n_p, because the hybridization increases with δ. Com-

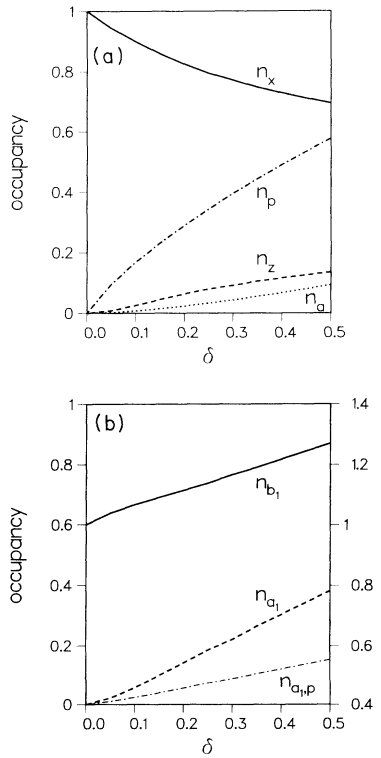

FIG. 7. Orbital occupancies as a function of doping in the insulating regime ($\Delta = 5$) for weak apex-plane coupling: $\varepsilon_a = 6$, $t'_{pd} = 0.4$, $t'_{pp} = 0.267$; all other parameters as in Table I (all the energies are in eV); meaning of lines as in Fig. 4.

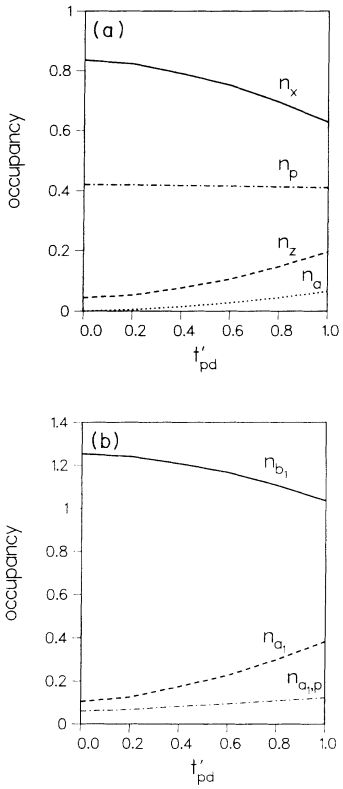

FIG. 8. Orbital occupancies vs apex-plane hopping matrix element in the insulating regime ($\Delta=5$) for $\varepsilon_a=6$ and $\delta=0.3$; all other parameters as in Table I; meaning of lines as in Fig. 4.

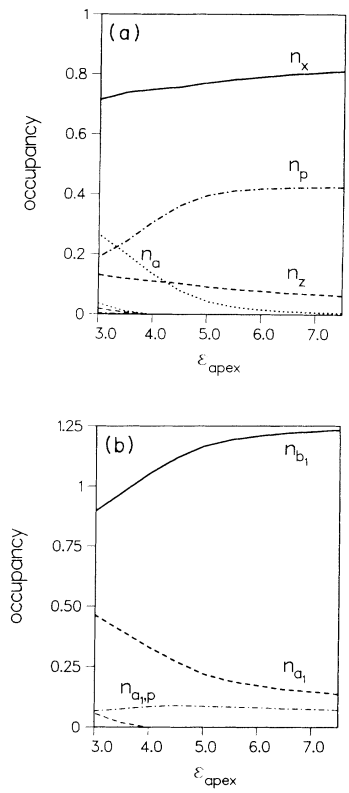

FIG. 9. Orbital occupancies vs apical oxygen orbital energy in the insulating regime ($\Delta=5$) for $t'_{pd}=0.4$, $t'_{pp}=0.267$, and $\delta=0.3$; all other parameters as in Table I; meaning of lines as in Fig. 4.

parison of Figs. 8 and 9 with Figs. 5 and 6 shows that, as regards the dependence on the apical parameters, the occupancies behave much the same as in the metallic regime, in particular when analyzed in terms of local a_1 vs b_1 symmetry. The changes with ε_a are somewhat larger, mainly because of a rapid increase in n_a at the expense of n_p when ε_a drops below ε_p.

C. Optical conductivity

We have also calculated the frequency-dependent conductivity from the current-current response function. The current matrix element in the x direction as obtained from the continuity equation is

$$J^x=J^x_{pd_x}+J^x_{pd_z}+J^x_{pp}+J^x_{pa}$$

$$=-\frac{e}{\hbar}at_{pd}b\sum_{k,\sigma}\cos(k_x/2)[(d^\dagger_x)_{k,\sigma}(p_x)_{k,\sigma}+\text{H.c.}]+\frac{e}{\hbar}\frac{at_{pd}b}{\sqrt{3}}\sum_{k,\sigma}\cos(k_x/2)[(d^\dagger_z)_{k,\sigma}(p_x)_{k,\sigma}+\text{H.c.}]$$

$$+\frac{e}{\hbar}2at_{pp}\sum_{k,\sigma}\beta_k[(p^\dagger_x)_{k,\sigma}(p_y)_{k,\sigma}+\text{H.c.}]+\frac{e}{\hbar}\sqrt{2}at'_{pp}\sum_{k,\sigma}\cos(k_x/2)[(p^\dagger_a)_{k,\sigma}(p_x)_{k,\sigma}+\text{H.c.}]\,, \tag{9}$$

with $\beta_k\equiv\cos(k_x/2)\sin(k_y/2)$. The contribution to the xx component of the (sheet) conductivity made by optical transitions between bands λ and λ' is then given by

$$\sigma^{xx}_{\lambda\lambda'}(\omega)=\frac{\pi}{N_c a^2}\sum_k\frac{|J^x_{\lambda\lambda'}|^2}{\omega}[f(E_\lambda(k))-f(E_{\lambda'}(k))]\delta(E_{\lambda'}(k)-E_\lambda(k)-\hbar\omega)\,, \tag{10}$$

where the Fermi function $f(\cdots)$ restricts the momenta such that $E_\lambda(k)<\varepsilon_F$ in band λ and $E_{\lambda'}(k)>\varepsilon_F$ in band λ'. The conductivity is related to the kinetic energy by the following sum rule:

$$\sum_{\lambda,\lambda'}\int_0^{+\infty}\text{Re}\sigma^{xx}_{\lambda\lambda'}(\omega)d\omega=-\frac{\pi}{16}\frac{e^2}{\hbar^2}(\langle T_{pd_x}\rangle+\langle T_{pd_z}\rangle+2\langle T_{pp}\rangle+\langle T_{pa}\rangle) \tag{11}$$

(again $E_\lambda \leq \varepsilon_F$; $E_{\lambda'} \geq \varepsilon_F$ in the averages expressed by the brackets), where the various T's are the contributions to the kinetic energy per unit cell coming from the various hybridizations, e.g.,

$$T_{pd_x} = -\frac{2t_{pd}b}{N_c} \sum_{k,\sigma} \{\sin(k_x/2)[(d_x^\dagger)_{k,\sigma}(p_x)_{k,\sigma} + \text{H.c.}] - \sin(k_y/2)[(d_x^\dagger)_{k,\sigma}(p_y)_{k,\sigma} + \text{H.c.}]\} \ . \tag{12}$$

The conductivity arising from the direct interband transition between the lowest two bands in the low-energy region is shown for some typical values of the doping in Fig. 10 (the intraband Drude peak at zero frequency is omitted) for the same metallic parameters as above and not too strong apex-plane interaction. One observes that the absorption peak is in the range of 1 eV, independent of doping. The area under the peak hardly changes with doping because the weight added upon increasing δ largely goes into transitions to the higher bands; the sum rule is satisfied though.

Again it is interesting to compare this with the behavior in the "insulating" regime, shown in Fig. 11, for the same insulating parameters and weak apex-plane interaction as above. The absorption peak is now near 0.5 eV, is narrower by about a factor 2, and moves to slightly higher frequencies with doping. The lower transition frequency and smaller width reflect the more insulating closer spacing and smaller dispersion of the bands. In this case the area under the peak roughly scales with doping because the weight in transitions to higher bands is relatively unimportant.

D. Peierls instability

We have seen that in the two-band situation the part of the Fermi surface associated with the lower band develops rather flat edges parallel to the k_x and k_y axes, and one might suspect that this could give rise to a Peierls instability. Within the context of the present model this can be investigated by the frozen-phonon method, where one varies the amplitude of the lattice mode that is expected to become unstable, recalculating the electronic structure and, in particular, the energy of the system for each value of the deformation. However, for realistic values of the doping, we are faced here with the difficulty that the phonon wave vector that is required to connect opposite edges of the Fermi surface would be considerably shorter than π/a, so that the unit cell of the deformed lattice would in general be very large. In order to enable us to study the Peierls problem at least semiquantitatively, we decided to make it tractable for calculation by considering a case where the doping is increased to such a high value (actually $\delta = 0.67$) that the connecting phonon wave vector is precisely on the zone boundary, i.e., corresponds only to cell doubling. The calculation is illustrated in Fig 12, which shows the band structure and the Fermi surface, first for the undistorted lattice [Figs. 12(a) and 12(c)], then for a finite deformation corresponding to the X-point semiquadrupolar mode in which the oxygen ions along the x axis are displaced alternatingly to the right and to the left [Figs. 12(b) and 12(d)]. We see how, indeed, a gap opens up at the new zone boundaries at $k_x = \pm\pi/2a$ (note that bands and surfaces are shown as appropriate for the new reduced Brillouin zone, but are extended over the full unreduced zone).

The results of the stability analysis are shown in Fig. 13. The upper curve corresponds to the parameter values estimated in the most straightforward way: an electron-lattice coupling strength $\bar{g} = 4t_{pd}$ and $\bar{g}_p = 3t_{pp}$, as would follow from a $1/r^4$ and $1/r^3$ distance dependence of the p-d and p-p hopping matrix elements, and a bare frequency of 80 meV for the semiquadrupolar mode amounting to a renormalized frequency of 72 meV. One sees that no lattice distortion would occur for these parameter values. The other curves in Fig. 13 are for increasing values of the p-d electron-lattice coupling, and show that the system is, nevertheless, not far from a Peierls instability: for $\bar{g} \approx 8.0$, which is only twice the estimated value, a finite

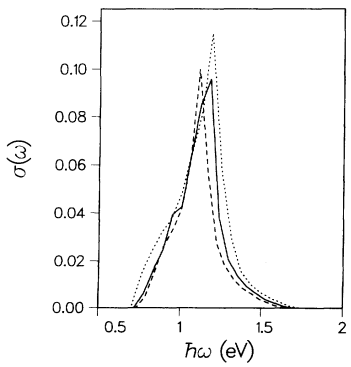

FIG. 10. Optical conductivity (in units of $e^2/\hbar$) vs frequency in the metallic regime ($\Delta = 3$) for weak apex-plane coupling [model parameters same as in Figs. 2(a) and 2(c)]; dashed line: $\delta = 0.1$, solid line: $\delta = 0.2$, dotted line: $\delta = 0.3$.

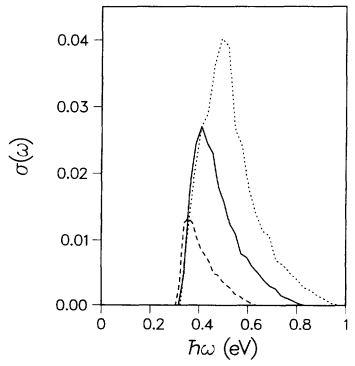

FIG. 11. Optical conductivity (in units of $e^2/\hbar$) vs frequency in the insulating regime ($\Delta = 5$) for weak apex-plane coupling (model parameters same as in Fig. 7); dashed line: $\delta = 0.1$, solid line: $\delta = 0.2$, dotted line: $\delta = 0.3$.

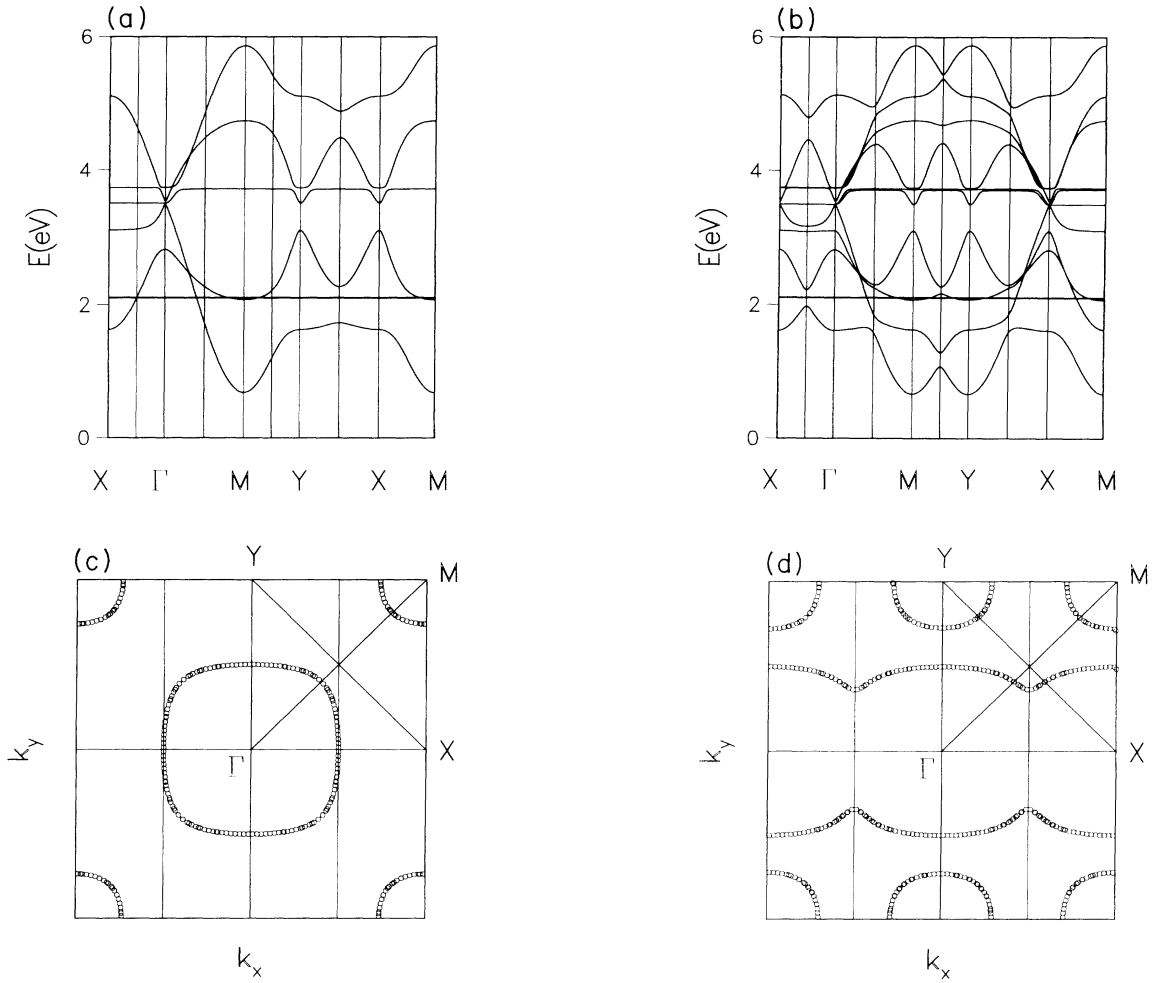

FIG. 12. Band structure (a) and (b) and Fermi surface (c) and (d) in the metallic regime ($\Delta=3$) for intermediate apex-plane coupling, $\varepsilon_a=3$, $t'_{pd}=0.4$, $t'_{pp}=0.267$, and large doping, $\delta=0.67$, and all other parameters as in Table I (all the energies are in eV); (a) and (c) for the undistorted square lattice, (b) and (d) for a semiquadrupolar X-point distortion $\bar{u}_X^{(sq)}=0.04$.

distortion would develop.

We should point out that, by increasing the doping to $\delta=0.67$, we have rounded off the inner Fermi surface considerably [compare Fig. 12(c) with Fig. 2(d)]. The fact that the system is then still rather close to a Peierls instability, although this would not occur for the estimated parameter values, indicates that, for lower and more realistic values of the doping, such an instability would be likely to occur in the two-band situation.

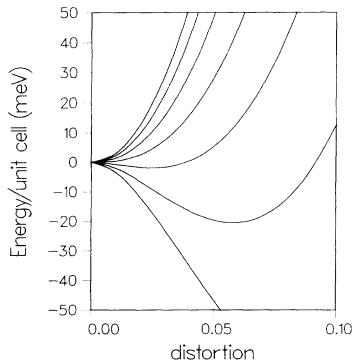

FIG. 13. Total energy vs semiquadrupolar X-point distortion for various values of the p-d electron-phonon coupling constant; the successive curves correspond to $\bar{g}$ being increased by steps of 1.0 from 4.0 (upper curve) to 10.0.

Actually, no lattice distortion of the type considered has been observed in the high-T_c compounds, consistent with our estimate that, in the hole-doped high-T_c cuprates, the actual positions of the energy levels and the values of the hybridization parameters do not allow the two-band situation to arise for realistic values of doping.

IV. COMPARISON WITH EXPERIMENTS

A. Photoemission

Angular-resolved photoemission spectroscopy (ARPES) and angular-resolved inverse photoemission spectroscopy (ARIPES) are a direct source of information on the electronic band structure, and therefore provide a first test on our results. It is usually claimed that the AR(I)PES data agree qualitatively with standard LDA band calculations. In particular, this is considered to support the hypothesis that the doped high-T_c oxides are in the Fermi-liquid regime. The very same conclusion

could be drawn as well from the agreement with our present model calculations. However, LDA calculations appear to describe poorly the strong local repulsions giving rise to the insulating behavior of the undoped materials, and as a consequence obtain too broad bands. On the other hand, our SBMF approach, being nonperturbative in the coupling constant U_d, is able to capture both the possibility of insulating behavior and of reduced bandwidths.

Nevertheless, one should be aware of two limitations contained in our simplified scheme. First, as already mentioned above, our single-slave-boson scheme is not able to describe the local (intracell) hybridization, which is present even in the insulating state of the cuprates, independently from the delocalization associated with band formation. It is therefore biased towards the metallic state and, consequently, the model system is expected to behave overly metallic unless one forces it towards more insulating behavior by taking a larger value for Δ than commonly estimated. Second, the tight-binding approximation, although widely used in this field, may fail to reproduce details of the band structure and thus lead to incorrect curvature of the Fermi surface.

Keeping this in mind, however, one recognizes that the general features of our calculated band structure are in good agreement with AR(I)PES experiments on $Bi_2Sr_2CaCu_2O_8$ (Bi2212).[60–64] [Note that the band structures in those experimental papers are plotted in the electron picture, upside down with respect to our hole picture; moreover, their labeling of special points in the Brillouin zone is for the (three-dimensional) face-centered tetragonal crystal structure, the correspondence with our labeling for the (two-dimensional) square-lattice structure being $\overline{M}(\text{fct}) \equiv X(\text{sq})$ and $X(\text{fct}) \equiv M(\text{sq})$; we shall switch to electron language and fct labeling for the remainder of this subsection.] In particular, we find that the intersections of the lowest band with the Fermi level agree closely with the crossing points observed experimentally: close to the $\overline{M}$ point along $\Gamma\overline{M}$, and about halfway (but closer to Γ) along ΓX. If we keep the (metallic) estimate for Δ, we obtain that the part of this band below E_F is about 1 eV wide, while the experimental ARPES bandwidth is less than 0.25 eV. However, the calculated width is reduced to about 0.3 eV if we use the larger value for Δ forcing the model into the insulating regime, suggesting that this might indeed be an appropriate way to compensate for the tendency towards metallic behavior of our SBMF approach.

An important issue is whether there are actually two bands at the Fermi surface, and, if so, what the nature of the second band is. This is also a delicate point experimentally because of the possibility that some of the broad features observed in ARPES do not originate from a quasiparticle band but should be attributed to an incoherent background. Consequently, the data on Bi2212, which do provide some indications for a multiple Fermi surface, have been interpreted in different ways: (i) two electron bands within 0.5 eV of E_F at the Γ point, both crossing E_F along ΓX and at least one of them doing so along $\Gamma\overline{M}$;[61,62] (ii) one electron band of about 0.25 eV width that crosses E_F along ΓX but remains below E_F along $\Gamma\overline{M}$, and a second band appearing precisely at the Fermi energy in the vicinity of the $\overline{M}$ point;[64] (iii) an electron band that crosses E_F along ΓX and a band (which may or may not be the same one) that crosses along $\Gamma\overline{M}$ near the $\overline{M}$ point and remains very close to E_F.[63]

From our present results we can make the following comments. That two bands are crossing the Fermi level [case (i)] appears to be rather unlikely, or more precisely, that both could be Cu-O-like Fermi-liquid quasiparticle bands: according to our calculations the situation where two such bands cross can, in principle, occur, but only for a very strong apex-plane interaction, which implies large values of $n_{a_1}(\delta) - \delta$, and as we shall see below (see Sec. V), that is expected to correspond to a low T_c or no superconductivity at all, quite contrary to Bi2212 having about the highest T_c observed; neither is it expected that the magnetic interactions, left out in the SBMF approach, could cause the a_1-like quasiparticle band to cross because those interactions are probably too weak, especially at intermediate doping, to produce such a global rearrangement of the band structure [which would lead, moreover, to drastic modifications of the densities of holes with different symmetries and could hardly preserve the remarkable correlation between $n_{a_1}(\delta) - \delta$, and $T_c^{\max}$ discussed below in Secs. V and VI]. Nevertheless, one could still speculate that the *local* correlations, which are beyond the present uniform mean-field approach, could distinguish and select on a local basis the various components with different symmetries in the quasiparticles. This could lead to the experimental observation of a two-component Fermi-liquid formed by heavy b_1 and lighter a_1 particles, thereby mimicking a two-band crossing. However, that is clearly outside the simple Fermi-liquid picture of the present treatment.

On the other hand, if the Fermi level is intersected only once both along ΓX and along $\Gamma\overline{M}$ [cases (ii) and (iii)], there are still two possibilities: (a) the crossing along ΓX is due to a hybridized Cu-O band, while that near $\overline{M}$ is due to a Bi-O band as predicted by LDA (Refs. 65-67) and suggested in Refs. 63 and 64, so that the Fermi surface is disconnected and the Cu-O part of it consists of large hole pockets centered around the X point, which the present approach fails to reproduce; (b) the crossings belong to the same Cu-O band and the Fermi surface is connected, an interpretation that is certainly allowed by the experimental data as pointed out in Ref. 63; our results suggest that this might actually be the case: the crossing Cu-O band would then be identified as the b_1-like lowest band, while the noncrossing band at higher binding energy would be the a_1-like band.

B. XAS and EELS

X-ray-absorption spectroscopy and electron-energy-loss spectroscopy provide additional information on the electronic structure since the total intensity of an absorption peak is a direct measure of the density of holes on a particular ion in a certain energy band. Information on the occupation of specific orbitals can be extracted from experiments on single crystals or well-oriented thin films by XAS with polarized radiation and from EELS at

different momentum transfers exploiting the selection rules. Of particular interest in the present case are polarized Cu L_3 XAS and Cu $2p_{3/2}$ EELS, where, from the relative intensity of $2p(\text{core}) \rightarrow 3d$ transitions at different polarizations, one obtains information on the relative density of holes in the Cu d_x and d_z orbitals, providing a direct connection with n_x and n_z calculated from our model. Also of interest are polarized O K-edge XAS and O $1s$ EELS, which provide information on the relative hole densities in oxygen $2p$ orbitals oriented perpendicular and parallel to the CuO_2 planes.

Both XAS (Ref. 3) and EELS,[4] as well as resonant photoemission,[61] indicate a dominant O $2p$ nature of the states near the Fermi level, apparently in conflict with the predominant Cu d_x character of the calculated b_1-like band. However, one should keep in mind that the coherence factor b^2 is directly related to the residue of the pole in the single-particle Green's function of the physical particles. Consequently, the measured Cu $3d$ weight is reduced by a factor $b^2 \approx 0.1$ with respect to the calculated d component in the band, while the measured O $2p$ weight does not involve the b^2 and is simply equal to the calculated p component. With this correction taken into account, our results correspond to an (O p)/ (Cu d) weight ratio of ≈ 6, in good agreement with the observed ($\approx 80\%$) p character. We also point out that the small value of b^2 signals the relevance of the correlations, which reduce the relative weight of the coherent pole with respect to the incoherent background.

The values for n_z calculated for intermediate apex-plane interaction [e.g., as in Fig. 4(a)] agree very well with the 10–20% range observed in XAS (Refs. 24 and 25) and EELS.[26,27] The reported variation of n_z/n_x with T_c for each individual compound,[24,25] assumed to be associated with an increase in total hole concentration, is also explained by our calculation as due to the increase in n_z with doping and the accompanying slight decrease in n_x. We point out that, for not too strong an apex-plane interaction, the calculated occupancy of the apical oxygen orbital itself remains rather small (less than a few percent), in agreement with the data from polarized XAS (Refs. 68 and 69) and EELS.[27]

C. Optical absorption

Optical reflectivity measurements show that the conductivity of all the high-T_c cuprates has a very broad peak in the mid-infrared region (≈ 0.5 eV), the so-called mid-infrared band.[70] It appears that this is not well represented by a Drude model, but is best accounted for by a separate broad Lorentzian contribution to the dielectric function which comes in addition to a Drude term. Although explanations in terms of frequency-dependent scattering mechanisms have also been put forward,[71,72] it is possibly due to a direct electronic transition.[70] According to the present analysis it could well be interpreted as the interband optical transition between the two low-lying p-d hybridized bands.[30] Although the peak in the optical absorption is at too high frequency when calculated for the "metallic" parameters (Fig. 10), it is shifted towards the observed frequency range (see Fig. 11) when we apply the same rescaling of Δ originally introduced in order to obtain "insulating" behavior at low doping, and which also yielded the correct order of magnitude for the bandwidths observed in ARPES. This lends additional support to the suggestion that such rescaling is a consistent procedure to compensate for the bias towards metallic behavior in the SBMF approach. We further point out that, because of the SBMF approach, the calculated spectra give only the coherent (quasiparticle) part of the optical conductivity. A noncoherent part is expected to appear as a background that will extend to higher frequency. This might explain the large linewidths occurring in the Lorentzian fits to the measured spectra.

V. RELATION BETWEEN ELECTRONIC STRUCTURE AND T_c

In Sec. III we have identified the total occupancy of states with local a_1 symmetry as a characteristic feature in the electronic structure that is strongly affected by the apical oxygen, and thus could differentiate between the various cuprates. In an attempt to find a relation between crystal structure, electronic structure, and high-T_c superconductivity, we therefore direct our attention towards the quantity n_{a_1}.

We have computed the parameters for ten representative cuprate compounds, with maximum critical temperatures ranging from 0 to 110 K, selected among those with the most reliable structural data compiled in Ref. 43. For each compound we have calculated n_{a_1} *at the optimum doping value* $\delta^{\max}$ for which the maximum critical temperature $T_c^{\max} = T_c(\delta^{\max})$ is attained in that compound. However, as seen in Fig. 14(a), there is no obvious correlation between $T_c^{\max}$ and $n_{a_1}(\delta^{\max})$. In an attempt to disentangle the effect of crystal structure on critical temperature from that of doping by correcting for the differences in optimum doping values between the compounds, we consider $n_{a_1}(\delta^{\max}) - \delta^{\max}$, the excess of holes with local a_1 symmetry with respect to the doping itself, again at the optimum doping value. Figure 14(b) shows $T_c^{\max}$ plotted versus this quantity and, as reported preliminarily,[44] it is evident that a well-defined trend exists: *the higher* $n_{a_1}(\delta^{\max}) - \delta^{\max}$ *is, the lower* $T_c^{\max}$ *is.* We have tried several alternatives but it appears that such a clear correlation with $T_c^{\max}$ shows up only for $n_{a_1}(\delta^{\max}) - \delta^{\max}$, or as one would expect, and shown also in Fig. 14(c), for the approximately complementary quantity $n_{b_1}(\delta^{\max}) - 1$, the excess of holes with local b_1 symmetry with respect to 1 (which is the value in the insulating limit at zero doping). We have further checked the robustness of the obtained correlation against a rescaling of the bare charge-transfer gap that shifts the parameters of all compounds into the insulating regime.

Concerning the relation between crystal structure and superconductivity, our results imply that $T_c^{\max}$ *is highest in compounds where the apex-plane interaction is weakest.* This can be appreciated from our earlier result (Sec. III B) that, for a *fixed* value of the doping, n_{a_1} decreases (and n_{b_1} increases) with decreasing apex-plane interac-

tion. The calculated variation of $n_{a_1}(\delta^{max})-\delta^{max}$ between the compounds is actually largely due to the variation in $\varepsilon_a-\varepsilon_p$, i.e., in the Madelung potential difference between the apical and the planar-oxygen ions, rather than to the variation in the apex-planar hopping integrals t'_{pd} and t'_{pp}, in agreement with the observation[43] that the compounds with the lowest ε_a have the lowest T_c^{max}.

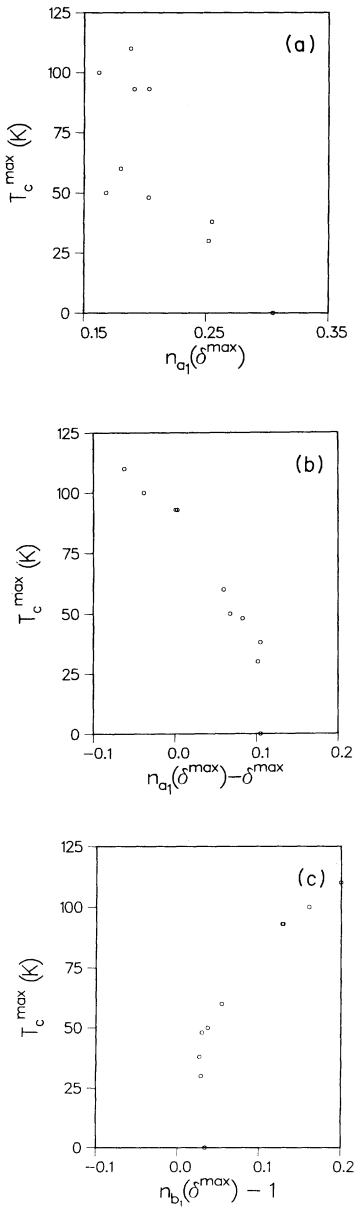

FIG. 14. Maximum critical temperature T_c^{max} of various superconducting cuprates vs (a) the corresponding density $n_{a_1}(\delta^{max})$ of holes with a_1 symmetry at the doping δ^{max} at which T_c^{max} is attained, (b) vs the excess density of a_1-symmetry holes $n_{a_1}(\delta^{max})-\delta^{max}$, (c) vs the excess density of b_1-symmetry holes $n_{b_1}(\delta^{max})-1$. The input parameters are obtained from Ref. 43 for the compounds $La_2SrCu_2O_6$ ($T_c^{max}=0$ K), $La_{1.85}Ba_{0.15}CuO_4$ ($T_c^{max}=30$ K), $La_{1.85}Sr_{0.15}CuO_4$ ($T_c^{max}=38$ K), $(Ba_{0.67}Eu_{0.33})_2(Eu_{0.67}Ce_{0.33})_2Cu_3O_{8.78}$ ($T_c^{max}=48$ K), $Y_{0.8}Ca_{0.2}Ba_2Cu_3O_{6.11}$ ($T_c^{max}=50$ K), $YBa_2Cu_3O_{6.5}$ ($T_c^{max}=60$ K), $YBa_2Cu_3O_7$ ($T_c^{max}=93$ K), $Bi_2Sr_2Ca_{0.9}Y_{0.1}Cu_2O_{8.24}$ ($T_c^{max}=93$ K), $TlBa_2CaCu_2O_7$ ($T_c^{max}=100$ K), $Pb_{0.5}Tl_{0.5}Sr_2CaCu_2O_7$ ($T_c^{max}=110$ K).

It is worth emphasizing again that it is *not* a large amount of a_1 holes by itself that is detrimental to superconductivity (no apparent correlation exists between n_{a_1} and T_c^{max}), but rather the excess of a_1 holes with respect to doping $n_{a_1}(\delta^{max})-\delta^{max}$, and, moreover, that the correlations found are between *maximum* critical temperature and occupancies *at optimum doping,* not between critical temperature and occupancies as such at arbitrary doping. This is, therefore, perfectly compatible with the observation[24,25] from polarized Cu L_3 XAS experiments that both n_z (which accounts for a large part of n_{a_1}) and T_c increase with doping *in any particular compound* when starting from the insulator. In contrast, our findings do not support the suggestion[24,25] that the occupation of the d_z orbital would be positively correlated with the value of T_c in general, also *between different compounds.* The picture suggested by our results is rather that, when in a particular cuprate T_c is raised by introducing holes starting from the undoped insulator, the increase in n_z is just an inevitable consequence of the *doping,* but that the maximum T_c that is then reached is highest in the compound where the *crystal structure* is such that this increase in n_z is kept as low as is compatible with the value of the doping, and this is the case if the apex-plane interaction is weak.

For the sake of completeness, we ought to mention that we have found no indication that the crossing of the Fermi level by the second band, which is the second feature that we found in Sec. III to be strongly dependent on the apex-planar interaction, is significant in relation to the occurrence of high-T_c superconductivity. For the parameter values pertinent to the actually existing cuprates,[43] even when rescaled to simulate more insulating behavior, such a second-band crossing does not occur for physically relevant values of the doping.

Finally, we should point out that the analysis performed with rescaling the bare parameters, while demonstrating a remarkable robustness in the general trend of T_c^{max} vs $n_{a_1}(\delta^{max})-\delta^{max}$ or T_c^{max} vs $n_{b_1}(\delta^{max})-1$, also showed that the absolute values of $n_{a_1}(\delta^{max})$ and $n_{b_1}(\delta^{max})$ are highly sensitive to such rescaling. The absolute scale along the horizontal axes in Fig. 14 is therefore not reliable, and it is not permitted to conclude that $n_{a_1}(\delta^{max})-\delta^{max}$ should be maximally negative [or $n_{b_1}(\delta^{max})-1$ maximally positive] in order to have the highest T_c^{max}. For example, it could well be that the optimum condition, reached in the highest-T_c compounds, is actually $n_{a_1}(\delta^{max})\approx\delta^{max}$ [or $n_{b_1}(\delta^{max})\approx 1$], and that larger values for $n_{a_1}(\delta^{max})$ [or smaller values for $n_{b_1}(\delta^{max})$] occur in the compounds with lower T_c.

VI. DISCUSSION

Finally, we want to point out some implications of our results for models and mechanisms that have been pro-

posed to explain the phenomenon of high-T_c superconductivity. Two main results have to be considered: (i) for reasonable values of the input parameters only one band crosses the Fermi level; (ii) the higher $n_{a_1}(\delta^{\max})-\delta^{\max}$ [or $1-n_{b_1}(\delta^{\max})$] is, the lower $T_c^{\max}$ is (with the proviso that the optimum absolute values of these quantities cannot be determined reliably).

The fact that we find that for acceptable values of the model parameters the holes are contained in a single band might be considered as a support for the adequacy of a single-band model, the t-J model in particular, to describe high-T_c superconductivity. However, the composite nature of the obtained band, the fact that it consists of orbitals of different local symmetry, asks for a more subtle consideration. The t-J model as derived by Zhang and Rice[7] requires the existence and the stability of the Zhang-Rice singlets, which consist entirely of b_1-symmetry orbitals. A high occupancy of a_1-symmetry orbitals therefore corresponds to a situation where the electronic structure is no longer adequately represented by the t-J model. The decrease of $T_c^{\max}$ and the subsequent disappearance of superconductivity with increasing $n_{a_1}(\delta^{\max})-\delta^{\max}$ would be perfectly compatible with the idea that the t-J model is the correct model for high-T_c superconductivity and that superconductivity disappears when the t-J model becomes invalid because the Zhang-Rice singlet is no longer kinetically stable. This is the same conclusion as obtained from the analysis of the nature of the low-lying states in Cu_2O_9 and Cu_2O_{11} clusters.[43] One should note that this implies that the relation between the structure of various systems and superconductivity is itself outside the scope of the t-J model, as is the change in symmetry of the holes with doping for a given system. It is then not so obvious that the t-J model is capable to describe the dependence of T_c on doping correctly. A further study into the conditions under which the t-J model can be derived from more realistic many-band models would certainly be of interest.

With respect to the Kondo-lattice model and similar two-band models,[13–19] the argument would rather be reversed. Insofar as these models presuppose two weakly interacting but distinct quasiparticle bands, one of light holes and another one of massive spins, such a picture is not directly supported by our findings where only a single quasiparticle hole band is found below the Fermi level for reasonable values of the parameters. One can now argue that, apart from the possibility of really having a crossing of the Fermi level by another band, a two-band description is actually required by the composite nature of this single hole band, where the flatter (i.e., more massive), lower, mostly b_1-like part represents the localized copper spin degrees of freedom, while the steeper, upper, mostly a_1-like part that intersects the Fermi level represents the mobile holes. One would assume that the local correlations omitted in the SBMF approach would separate these parts and, moreover, lead to antiferromagnetic correlations between the copper spins. We work now on the assumption that the superconductivity is carried by the mobile holes and arises from their interaction with the "substrate" of locally antiferromagnetically correlated Cu spins. Then our findings concerning $T_c^{\max}$ and the occupancies could be quite naturally interpreted as expressing that the pairing potential provided by the substrate is stronger in a system where doping a sufficient number of holes into the carrier band is accompanied by a smaller reduction of n_{b_1}, i.e., it produces less damage to the substrate, which is correlated most effectively when $n_{b_1}=1$. This would be compatible with the idea that the Kondo-lattice model contains the essential physics required for high-T_c superconductivity, and that, where the model loses its validity, superconductivity disappears. Again, one should note that the relation between structure and superconductivity is outside the scope of the model. Nevertheless, we should emphasize that our present analysis provides no direct indication for a strict separation of (Cu) spins and (O) carriers, but rather suggests a two-band model where two local states of different symmetry appear on a more or less equal footing.

Several excitonic mechanisms have been proposed that make use of the Coulomb interactions to produce superconductive pairing: either by charge-transfer fluctuations[6,73] involving the Cu-O nearest-neighbor Coulomb repulsion V_x (or V_z), or by crystal-field fluctuations[74,75] involving V_x-V_z, or by d-d excitations[28,29] involving the off-diagonal Coulomb interaction V_{xz}. Since these interactions are contained in the present model [the off-diagonal interaction was omitted in Eq. (1) because it does not contribute in lowest order], the effect of such fluctuations would actually appear in higher order in the $1/N$ expansion of which the present SBMF treatment is the zeroth order. It is interesting to note that the expected behavior of these Coulomb excitonic mechanisms is quite compatible with our findings concerning $T_c^{\max}$. For the charge-transfer mechanism, the strongest interaction of a hole on planar oxygen is with a hole in the Cu d_x orbital ($V_x > V_z$). Since a high value of $n_{a_1}(\delta^{\max})-\delta^{\max}$ corresponds to a large occupancy of d_z at the expense of the occupancy of d_x, it implies an effectively reduced Cu-O nearest-neighbor Coulomb interaction and, consequently, a reduced pairing potential due to the charge-transfer modes. For the crystal-field mechanism, the relevant quantity is actually the difference between the value of $V_x\langle n_{xi}\rangle + V_z\langle n_{zi}\rangle$ in the ground state and in the crystal-field excited state (which equals V_x-V_z in the simplest case,[74,75] where the Cu hole is in d_{xi} in the ground state and in d_{zi} in the excited state). Larger n_{a_1} and smaller n_{b_1} amount to larger $\langle n_{zi}\rangle$ and smaller $\langle n_{xi}\rangle$ in the ground state, and correspondingly smaller $\langle n_{zi}\rangle$ and larger $\langle n_{xi}\rangle$ in the excited state, implying the relevant difference to be smaller and the pairing potential to become weaker, consistent with a lower $T_c^{\max}$. The strength of the d-d mechanism depends upon the size of the matrix element of $d_{zi}^{\dagger}d_{xi}$ between the lowest two bands. Since larger n_{a_1} and smaller n_{b_1} corresponds to stronger mixing between the different local symmetries, making the lowest (second) band less purely b_1 (a_1), this is expected to imply a diminished matrix element, again consistent with a lower $T_c^{\max}$. To see whether these sim-

ple considerations are really applicable would require a more detailed analysis.

VII. CONCLUSIONS

We have investigated the influence of the apical oxygen ion(s) on the electronic structure of a CuO_2 plane. This has been done in a band-structure approach which emphasizes the gain in kinetic energy associated with delocalization, and it is complementary to a cluster approach which emphasizes the local correlations. The approach assumes that the system is in a Fermi-liquid regime, which is expected to apply at not too low doping levels. The band structure is calculated within a tight-binding scheme, with the correlations on the copper ions treated by a slave-boson method in mean-field approximation and the copper-oxygen Coulomb repulsions in Hartree approximation.

We have made a systematic investigation of the variation of various physically relevant properties with variation of the parameters that determine the coupling of the apical oxygen to the CuO_2 plane: the energy level of the apical oxygen orbital and the hopping integrals between the apical oxygen and the plane. The results show that, if the bare energy level gets close to or below that of the planar oxygens and/or the copper-apical hopping matrix element is sufficiently large, the hole occupancy n_z of the copper d_z orbitals (and of the oxygen orbitals of the same local a_1 symmetry, which includes the apex orbital) is strongly enhanced at the expense of the occupancy of the copper d_x orbitals (and the oxygen orbitals of the same b_1 symmetry). For fixed model parameters, the d_z occupancy increases slightly with doping, which is in agreement with what is observed in polarized Cu L_3 XAS experiments. Furthermore, for high doping level, two bands cross the Fermi level. It is found that the critical value above which this occurs decreases strongly with increasing coupling between the apical oxygen and the plane. We find that once this two-band situation occurs, the system might show a Peierls instability involving displacements of the oxygen ions in the CuO_2 plane.

Calculations performed for parameters pertinent to different cuprates indicate that the weaker the involvement of the apical oxygen, the higher is the value of $T_c^{\max}$ which can be reached at the optimum doping $\delta^{\max}$. However, this is by no means equivalent to the statement that a large n_{a_1} is by itself detrimental to superconductivity: it rather turns out that the occupancy of d_z orbitals (and other orbitals of a_1 local symmetry) is *not* correlated with $T_c^{\max}$. A clear correlation with $T_c^{\max}$ is, instead, found for the excess of a_1 holes with respect to doping $n_{a_1}(\delta^{\max})-\delta^{\max}$ or for the complementary quantity $n_{b_1}(\delta^{\max})-1$.

Thus superconductivity is favored either (i) when $n_{a_1}(\delta^{\max})-\delta^{\max}$ is as small (possibly negative) as possible [and $n_{b_1}(\delta^{\max})-1$ as large as possible], or (ii) when $n_{a_1}(\delta^{\max})$ is as close to $\delta^{\max}$ [and $n_{b_1}(\delta^{\max})$ as close to the value 1] as possible. The first alternative would be consistent with the interpretation that high-T_c superconductivity disappears once the low-energy physics can no longer be represented by a single-band $(t-J)$ model (based on orbitals with b_1 symmetry), as was previously concluded by Ohta *et al.*[43] on the basis of cluster calculations. However, also in the case of pairing mechanisms based on Coulombic repulsions, superconductivity would be favored by the a_1 hole occupancy being small. The second alternative would indicate that high-T_c superconductivity is associated with the low-energy physics of a two-band (Kondo-lattice) model where the doped holes go into a_1 orbitals leaving the b_1 "substrate" undisturbed. This suggests that one of these two models might contain the essential physics for high-T_c superconductivity (e.g., the pairing mechanism), but that a theory able to describe both doping dependence and the relation with crystal structure would require a more flexible two-band model where the two local states are on a more or less equal footing.

Our analysis has thus established a link between the crystal structure on the one hand and high-T_c superconductivity on the other hand via a particular feature in the electronic structure. Independently of how stringent our results are as far as the theoretical models are concerned, they thereby provide an indication which aspects of the electronic structure of the cuprates are relevant. In particular, our analysis shows that most simplified models, even though they could describe superconductivity, can hardly account for the differences among the various cuprates and for the doping dependence of T_c within each compound. For that purpose more detailed aspects of the electronic and crystal structures must be taken into consideration. A direct experimental corroboration (or refutation) of the proposed connection between electronic structure and high-T_c superconductivity would be most welcome. Most appropriate would be more extensive measurements by polarized XAS or EELS of the various occupancies as a function of doping on well-characterized samples of compounds with different $T_c^{\max}$.

ACKNOWLEDGMENTS

We would like to thank Professor C. Castellani, Professor A. Bianconi, and Professor M. F. H. Schuurmans for many interesting discussions and suggestions. This work has been supported by the European Economic Community under Contract No. SC1* 0222-C(EDB). M. G. also acknowledges partial support by Progetto SAT of the "Consorzio Interuniversitario di Fisica della Materia" (INFM).

APPENDIX

In this appendix we will provide a more detailed description of the mean-field procedure used in the present paper.

The Hamiltonian in Eq. (1) is modified by the introduction of the slave-boson fields by means of the replacement of the d and $d^\dagger$ operators

$$d^\dagger_{\alpha i,\sigma}\rightarrow d^\dagger_{\alpha i,\sigma}b_i,\quad d_{\alpha i,\sigma}\rightarrow b_i^\dagger d_{\alpha i,\sigma}\quad (\text{where } \alpha=x,z)\ ,$$

and is enlarged by the introduction of the constraint $b_i^\dagger b_i+n_{xi}+n_{zi}=1$, where $n_{xi}\equiv\sum_\sigma n_{xi\sigma}$ and $n_{zi}\equiv\sum_\sigma n_{zi\sigma}$

are the densities on site i of d_x and d_z holes, respectively. The constraint is then implemented by a Lagrange multiplier field λ_i. At the mean-field level, the boson fields b_i and λ_i are constant numbers b and λ, respectively. Whereas b multiplicatively renormalizes the p-d hopping terms, λ additively shifts the atomic levels of the d orbitals.

The V terms are decoupled via independent Hubbard-Stratonovich transformations which introduce eight complex pairwise conjugate auxiliary fields. In mean-field approximation these fields are then set to their constant mean-field value. For instance, from the V_x term one has

$$\begin{aligned} H_V^x &= V_x \sum_{\substack{i,j,\sigma,\sigma' \\ (\nu=x,y)}} [d^\dagger_{xi,\sigma} d_{xi,\sigma}][p^\dagger_{\nu j,\sigma'} p_{\nu j,\sigma'}] \\ &\equiv V_x \sum_i n_{xi}[2n_{pi}] \\ &= \sum_i \left[\frac{1}{V_x}|v_0|^2 + v_0^* n_{xi} - 2v_0 n_{pi} \right] , \end{aligned}$$

where $2n_{pi} \equiv \sum_{j(i),\sigma} n_{p_\nu j\sigma}$ (the sum extending over the sites neighboring site i). A similar procedure can be used for the V_z, V_x', and V_z' terms, which are decoupled by the fields u_0, w_0, and z_0 (and the related complex conjugate fields), respectively. Of course, these fields are not all independent, being related to the various densities of holes in the various orbitals

$$\langle n_{pi} \rangle = \frac{1}{2V_x} v_0^* = \frac{1}{2V_z} u_0^* , \quad \langle n_{ai} \rangle = \frac{1}{V_x'} w_0^* = \frac{1}{V_z'} z_0^* , \tag{A1}$$

$$\langle n_{zi} \rangle = -\frac{1}{V_z} u_0 = -\frac{1}{V_z'} z_0 , \langle n_{xi} \rangle = -\frac{1}{V_x} v_0 = -\frac{1}{V_x'} w_0 .$$

The above relations lead to the following equalities:

$$\begin{aligned} z_0^* &= \frac{V_z'}{V_x'} w_0^* , \quad z_0 = \frac{V_z'}{V_z} u_0 , \\ w_0 &= \frac{V_x'}{V_x} v_0 , \quad u_0^* = \frac{V_z}{V_x} v_0^* . \end{aligned} \tag{A2}$$

At the mean-field level the introduction of the Hubbard-Stratonovich decoupling is equivalent to the Hartree mean-field approach and results in a shift of the atomic levels of the p and d orbitals:

$$\begin{aligned} \bar{\varepsilon}_{d_x} &= \varepsilon_{d_x} + \lambda + v_0^* + w_0^* = \varepsilon_{d_x} + \lambda + 2V_x n_p + V_x' n_a , \\ \bar{\varepsilon}_{d_z} &= \varepsilon_{d_z} + \lambda + u_0^* + z_0^* = \varepsilon_{d_z} + \lambda + 2V_z n_p + V_z' n_a , \\ \bar{\varepsilon}_p &= \varepsilon_p - 2(u_0 + v_0) = \varepsilon_p + 2V_x n_x + 2V_z n_z , \\ \bar{\varepsilon}_a &= \varepsilon_a - (w_0 + z_0) = \varepsilon_a + V_x' n_x + V_z' n_z . \end{aligned} \tag{A3}$$

With the above mean-field approximations for b, λ, and for the Hubbard-Stratonovich fields one can define a free energy of the form

$$F = N_c \left[\lambda(b^2-1) + \frac{|v_0|^2}{V_x} + \frac{|u_0|^2}{V_z} + \frac{|w_0|^2}{V_x'} + \frac{|z_0|^2}{V_z'} - \frac{2k_B T}{N_c} \sum_{k,l} \ln(1 + e^{[\mu - E_l(k)]/k_B T}) \right] , \tag{A4}$$

where $E_l(k)$ are the bands of the system obtained by diagonalizing, for each point in k space, the Hamiltonian matrix

$$H_{k\sigma} = \begin{bmatrix} \bar{\varepsilon}_{d_x} & 0 & -2bt_{pd}\sin(k_x/2) & 2bt_{pd}\sin(k_y/2) & 0 \\ 0 & \bar{\varepsilon}_{d_z} & \frac{2bt_{pd}}{\sqrt{3}}\sin(k_x/2) & \frac{2bt_{pd}}{\sqrt{3}}\sin(k_y/2) & \frac{-4bt_{pd}'}{\sqrt{6}} \\ -2bt_{pd}\sin(k_x/2) & \frac{2bt_{pd}}{\sqrt{3}}\sin(k_x/2) & \bar{\varepsilon}_p & 4t_{pp}\alpha_k & 2\sqrt{2}t_{pp}'\sin(k_x/2) \\ 2bt_{pd}\sin(k_y/2) & \frac{2bt_{pd}}{\sqrt{3}}\sin(k_y/2) & 4t_{pp}\alpha_k & \bar{\varepsilon}_p & 2\sqrt{2}t_{pp}'\sin(k_y/2) \\ 0 & \frac{-4bt_{pd}'}{\sqrt{6}} & 2\sqrt{2}t_{pp}'\sin(k_x/2) & 2\sqrt{2}t_{pp}'\sin(k_y/2) & \bar{\varepsilon}_a \end{bmatrix} , \tag{A5}$$

where the diagonal elements (effective atomic levels) are given by the expressions of Eqs. (A3), and $\alpha_k \equiv \sin(k_x/2)\sin(k_y/2)$. In this notation the mean-field Hamiltonian can be written as[47]

$$H = \sum_{k,\sigma} ((d_x^\dagger)_{k\sigma} \; (d_z^\dagger)_{k\sigma} \; (p_x^\dagger)_{k\sigma} \; (p_y^\dagger)_{k\sigma} \; (p_a^\dagger)_{k\sigma}) \; H_{k\sigma} \begin{bmatrix} (d_x)_{k\sigma} \\ (d_z)_{k\sigma} \\ (p_x)_{k\sigma} \\ (p_y)_{k\sigma} \\ (p_a)_{k\sigma} \end{bmatrix} . \tag{A6}$$

It must be remembered that not all the mean-field parameters are independent [see Eqs. (A2)] and it should be noted that the use of the constraint $n_x+n_z=1-b^2$ and of the total number of particle condition $n_x+n_z+n_p+n_a=1+\delta$ further reduces the number of independent parameters to be self-consistently determined.

To determine the self-consistency equations, one has to find the stationary points of the free energy obtaining

$$\frac{\partial F}{\partial X}=\sum_{k,\alpha,i,j} f[E_\alpha(k)]U^\dagger_{\alpha i}(k)\left[\frac{\partial H}{\partial X}\right]_{ij}U_{j\alpha}(k)=0\ ,$$

where X indicates the independent mean-field parameter (e.g., b, λ, v_0, and w_0^*), the U's are the matrices which diagonalize the Hamiltonian at a given point in k space, and $f(\cdots)$ is the Fermi function.

More explicitly, the self-consistency equations are

$$\frac{\partial F}{\partial \lambda}=\sum_{k,\sigma}(\langle(d_x^\dagger)_{k,\sigma}(d_x)_{k,\sigma}\rangle+\langle(d_z^\dagger)_{k,\sigma}(d_z)_{k,\sigma}\rangle)+N_c(b^2-1)=0\ , \tag{A7}$$

$$\begin{aligned}\frac{\partial F}{\partial b}=&2\lambda bN_c-2t_{pd}\sum_{k,\sigma}\left[\sin(k_x/2)[\langle(d_x^\dagger)_{k,\sigma}(p_x)_{k,\sigma}\rangle+\text{c.c.}]-\sin(k_y/2)[\langle(d_x^\dagger)_{k,\sigma}(p_y)_{k,\sigma}\rangle+\text{c.c.}]\right]\\&+\frac{2t_{pd}}{\sqrt{3}}\sum_{k,\sigma}\left[\sin(k_x/2)[\langle(d_z^\dagger)_{k,\sigma}(p_x)_{k,\sigma}\rangle+\text{c.c.}]+\sin(k_y/2)[\langle(d_z^\dagger)_{k,\sigma}(p_y)_{k,\sigma}\rangle+\text{c.c.}]\right]\\&-\frac{4t'_{pd}}{\sqrt{6}}\sum_{k,\sigma}[\langle(d_z^\dagger)_{k,\sigma}(p_a)_{k,\sigma}\rangle+\text{c.c.}]=0\ ,\end{aligned} \tag{A8}$$

$$\frac{\partial F}{\partial v_0^*}=\sum_{k,\sigma}\langle(d_x^\dagger)_{k,\sigma}(d_x)_{k,\sigma}\rangle+\frac{N_c}{V_x}v_0=0\ , \tag{A9}$$

$$\frac{\partial F}{\partial w_0}=-\sum_{k,\sigma}\langle(p_a^\dagger)_{k,\sigma}(p_a)_{k,\sigma}\rangle+\frac{N_c}{V'_x}w_0^*=0\ . \tag{A10}$$

Solving these coupled equations together with the condition

$$\frac{\partial F}{\partial \mu}=-N_c(1+\delta)\ , \tag{A11}$$

fixing to $\frac{1}{2}(1+\delta)$ (δ is the doping with respect to half-filling) the number of holes per spin per cell, one obtains the required set of self-consistent mean-field parameters. Inserting these values back in the Hamiltonian it is finally possible to get the self-consistent band structure given by the eigenvalues $E_l(k)$.

In the case of a frozen-phonon calculation, the self-consistency equation (A8) is supplemented by the following extra terms coming from the electron-phonon interaction:

$$\begin{aligned}\cdots&+g\sum_{q,s}\eta_s^x(q)u_q^{(s)}\sum_{k,\sigma}\sin(k_x/2)[\langle(d_x^\dagger)_{k+q,\sigma}(p_x)_{k,\sigma}\rangle+\text{c.c.}]\\&-g\sum_{q,s}\eta_s^y(q)u_q^{(s)}\sum_{k,\sigma}\sin(k_y/2)[\langle(d_x^\dagger)_{k+q,\sigma}(p_y)_{k,\sigma}\rangle+\text{c.c.}]\\&-\frac{g}{\sqrt{3}}\sum_{q,s}\eta_s^x(q)u_q^{(s)}\sum_{k,\sigma}\sin(k_x/2)[\langle(d_z^\dagger)_{k+q,\sigma}(p_x)_{k,\sigma}\rangle+\text{c.c.}]\\&-\frac{g}{\sqrt{3}}\sum_{q,s}\eta_s^y(q)u_q^{(s)}\sum_{k,\sigma}\sin(k_y/2)[\langle(d_z^\dagger)_{k+q,\sigma}(p_y)_{k,\sigma}\rangle+\text{c.c.}]+\cdots\ .\end{aligned} \tag{A12}$$

---

[1]Proceedings of the International Conference M^{2}S HTSC II, Stanford, 1989, edited by R. N. Shelton, W. A. Harrison, and N. E. Phillips [Physica C **162-164**, (1989)]; *Strongly Correlated Electron Systems,* Proceedings of the Anniversary Adriatico Research Conference and Workshop, edited by G. Baskaran, A. E. Ruckenstein, E. Tosatti, and Y. Lu, Progress in High Temperature Superconductivity Vol. 23 (World Scientific, Singapore, 1990).

[2]J. G. Bednorz and K. A. Müller, Z. Phys. B **64**, 189 (1986).

[3]P. Kuiper, G. Kruizinga, J. Ghijsen, M. Grioni, G. A. Sawatzky, P. J. W. Weijss, F. H. M. de Groot, H. Verweij, L. F. Feiner, and H. Petersen, Phys. Rev. B **38**, 6483 (1988).

[4]N. Nücker, J. Fink, J. C. Fuggle, P. J. Durham, and W. M. Temmerman, Phys. Rev. B **37**, 5158 (1988).

[5]V. J. Emery, Phys. Rev. Lett. **58**, 2794 (1987).

[6]C. M. Varma, S. Schmitt-Rink, and E. Abrahams, Solid State

Commun. **62**, 681 (1987).
[7]F. C. Zhang and T. M. Rice, Phys. Rev. B **37**, 3759 (1988).
[8]H. Eskes and G. A. Sawatzky, Phys. Rev. Lett. **61**, 1415 (1988).
[9]H. Eskes, G. A. Sawatzky, and L. F. Feiner, Physica C **160**, 424 (1989).
[10]E. B. Stechel and D. R. Jennison, Phys. Rev. B **38**, 4632 (1988).
[11]P. W. Anderson, Science **235**, 1196 (1987); P. W. Anderson, in *Frontiers and Borderlines in Many Particle Physics,* Proceedings of the International School of Physics "Enrico Fermi," edited by J. R. Schrieffer and R. A. Broglia (North-Holland, Amsterdam, 1987), p. 1.
[12]V. J. Emery and G. Reiter, Phys. Rev. B **38**, 4547 (1988).
[13]W.-M. Que and G. Kirczenow, Solid State Commun. **64**, 1063 (1987).
[14]C. Castellani, C. Di Castro, and M. Grilli, Physica C **153-155**, 1659 (1988); Int. J. Mod. Phys. B **1**, 659 (1988); N. Cancrini, S. Caprara, C. Castellani, C. Di Castro, M. Grilli, and R. Raimondi, Europhys. Lett. **14**, 597 (1991).
[15]A. Aharony, R. J. Birgenau, A. Coniglio, M. A. Kastner, and H. E. Stanley, Phys. Rev. Lett. **60**, 1330 (1988).
[16]P. Prelovšek, Phys. Lett. A **126**, 287 (1987).
[17]H. Kamimura, S. Matsuno, and R. Saito, Solid State Commun. **67**, 363 (1988); H. Kamimura, Int. J. Mod. Phys. B **1**, 699 (1988).
[18]N. Andrei and P. Coleman, Phys. Rev. Lett. **62**, 595 (1989).
[19]J. Zaanen and A. M. Oleś, Phys. Rev. B **37**, 9423 (1988).
[20]A. Fujimori, Phys. Rev. B **39**, 793 (1989).
[21]J. F. Annett, R. M. Martin, A. K. McMahan, and S. Satpathy, Phys. Rev. B **40**, 2620 (1989).
[22]J. B. Grant and A. K. McMahan, Phys. Rev. Lett. **66**, 488 (1991).
[23]H. Eskes and G. A. Sawatzky, Phys. Rev. B **44**, 9656 (1991).
[24]A. Bianconi, P. Castrucci, A. Fabrizi, M. Pompa, A. M. Flank, P. Lagarde, H. Katayama-Yoshida, and G. Calestani, Physica C **162-164**, 209 (1989); in *Earlier and Recent Aspects of Superconductivity,* edited by J. G. Bednorz and K. A. Müller, Springer Series in Solid State Sciences Vol. 90 (Springer-Verlag, Berlin, 1990), p. 407.
[25]A Bianconi, in *Proceedings of the International Conference on Superconductivity-ICSC, Bangalore, 1990,* edited by S. K. Joshi, C. N. R. Rao, and S. V. Subranyam (World Scientific, Singapore, 1990), p. 448.
[26]H. Romberg, N. Nücker, M. Alexander, J. Fink, D. Hahn, T. Zetterer, H. H. Otto, and K. F. Renk, Phys. Rev. B **41**, 2609 (1990).
[27]N. Nücker, H. Romberg, X. X. Xi, J. Fink, B. Gegenheimer, and Z. X. Zhao, Phys. Rev. B **39**, 6619 (1989).
[28]W. Weber, Z. Phys. B **70**, 323 (1988).
[29]D. L. Cox, M. Jarrell, C. Jayaprakash, H. R. Krishna-murthy, and J. Deisz, Phys. Rev. Lett. **62**, 2188 (1989).
[30]M. Grilli, C. Castellani, and C. Di Castro, Phys. Rev. B **42**, 6233 (1990).
[31]K. I. Kugel' and D. I. Khomskiĭ, Usp. Fiz. Nauk **136**, 621 (1982) [Sov. Phys. Usp. **25**, 231 (1982)].
[32]J. Zaanen, A. M. Oleś, and L. F. Feiner, in *Dynamics of Magnetic Fluctuations in High T_c Superconductors,* Vol. 246 of NATO Advanced Study Institute, Series B: Physics, edited by G. Reiter, P. Horsch, and G. Psaltakis (Plenum, New York, 1991).
[33]L. F. Feiner and J. Zaanen, in *Electronic Properties of High-T_c Superconductors and Related Compounds,* edited by H. Kuzmany, M. Mehring, and J. Fink, Springer Series in Solid State Sciences Vol. 99 (Springer-Verlag, Berlin, 1990), p. 357.
[34]A. M. Oleś, J. Zaanen, and V. Drchal, in *Strongly Correlated Electron Systems II,* Proceedings of the Adriatico Research Conference and Miniworkshop, edited by G. Baskaran, A. E. Ruckenstein, E. Tosatti, and Y. Lu, Progress in High-Temperature Superconductivity Vol. 29 (World Scientific, Singapore, 1991), p. 131.
[35]C. Thomsen, M. Cardona, B. Gegenheimer, R. Liu, and A. Simon, Phys. Rev. B **37**, 9860 (1988).
[36]A. R. Bishop, R. L. Martin, K. A. Müller, and Z. Tesanović, Z. Phys. B **76**, 17 (1989).
[37]M. Frick, W. von der Linden, I. Morgenstern, and H. de Raedt, Z. Phys. B **81**, 327 (1990).
[38]M. Frick, I. Morgenstern, and W. von der Linden, Z. Phys. B **82**, 339 (1991).
[39]K. A. Müller, Z. Phys. B **80**, 193 (1990).
[40]J. Mustre de Leon, S. D. Conradson, I. Batistič, and A. R. Bishop, Phys. Rev. Lett. **65**, 1675 (1990).
[41]D. M. de Leeuw, W. A. Groen, L. F. Feiner, and E. E. Havinga, Physica C **166**, 133 (1990).
[42]Y. Ohta, T. Tohyama, and S. Maekawa, Physica C **166**, 385 (1990).
[43]Y. Ohta, T. Tohyama, and S. Maekawa, Phys. Rev B **43**, 2968 (1991).
[44]C. Di Castro, L. F. Feiner, and M. Grilli, Phys. Rev. Lett. **66**, 3209 (1991).
[45]The cases of one or two apical oxygen ions can be considered on equal footing: in the case of two (above and below the CuO_2 planes) apical oxygens, a single bonding combination of $2p_z$ orbitals hybridizes with the plane, whereas a nonbonding combination can be factorized out. For this reason the Hamiltonians for the one or two apical oxygen(s) only differ by a $\sqrt{2}$ normalization factor which rescales the plane-apical ions hopping integrals; Eq. (1) corresponds to the case of one apical oxygen ion.
[46]The present phase convention is different from that in Ref. 44.
[47]In defining the Fourier-transformed operators, a factor i has been absorbed into $(p_x)_{k,\sigma}$ and $(p_y)_{k,\sigma}$ in order to have real coefficients in the Hamiltonian.
[48]Although the local repulsion on oxygen sites U_p is sizable ($\approx$4–6 eV), it can be treated in Hartree approximation due to the small occupancy of oxygen orbitals per spin and per cell. We checked that the inclusion of this interaction does not affect our results but only amounts to a slight reduction of the oxygen occupancies.
[49]S. E. Barnes, J. Phys. F **6**, 1375 (1976); P. Coleman, Phys. Rev. B **29**, 3035 (1984); N. Read and D. M. Newns, J. Phys. C **16**, 3273 (1983); N. Read, *ibid.* **18**, 2651 (1985); A. J. Millis and P. A. Lee, Phys. Rev. B **35**, 3394 (1987); G. Kotliar and A. E. Ruckenstein, Phys. Rev. Lett. **57**, 1362 (1986).
[50]G. Kotliar, P. A. Lee, and N. Read, Physica C **153-155**, 538 (1988).
[51]M. Grilli, G. Kotliar, and A. J. Millis, Phys. Rev. B **42**, 329 (1990).
[52]H. Eskes, L. H. Tjeng, and G. A. Sawatzky, Phys. Rev. B **41**, 288 (1990).
[53]M. S. Hybertsen, M. Schlüter, and N. E. Christensen, Phys. Rev. B **39**, 9028 (1989).
[54]A. K. McMahan, R. M. Martin, and S. Satpathy, Phys. Rev. B **38**, 6650 (1988).
[55]L. H. Tjeng, J. van Elp, P. Kuiper, and G. A. Sawatzky, (unpublished); G. A. Sawatzky, in *Earlier and Recent Aspects of Superconductivity,* edited by J. G. Bednorz and K. A. Müller, Springer Series in Solid State Sciences Vol. 90 (Springer-Verlag, Berlin, 1990), p. 345.

[56]W. A. Harrison, *Electronic Structure and the Properties of Solids* (Freeman, San Francisco, 1980).

[57]The model could be made more realistic by clamping the CuO_2 plane between stiff elastic layers (representing, e.g., the La_2O_2 layers in La_2CuO_4) in which the apical oxygens are absorbed, but such improvement is unnecessary for the purpose of the present paper.

[58]L. Pintschovius, N. Pyka, W. Reichardt, A. Y. Rumiantsev, A. Ivanov, and N. Mitrofanov, in *International Seminar on High Temperature Superconducitivity, Dubna, 1989,* edited by V. L. Aksenov, N. N. Bogolubov, and N. M. Plakida, Progress in High-Temperature Superconductivity Vol. 21 (World Scientific, Singapore, 1990), p. 36.

[59]W. Reichardt, N. Pyka, L. Pintschovius, B. Hennion, and G. Collin, Physica C **162-164**, 464 (1989).

[60]G. Mante, R. Claessen, T. Buslaps, S. Harm, R. Manzke, M. Skibowski, and J. Fink, Z. Phys. B **80**, 181 (1990).

[61]T. Takahashi, H. Matsuyama, K. Kamiya, T. Watanabe, K. Seki, H. Katayama-Yoshida, S. Sato, and H. Inokuchi, Nature **334**, 691 (1988); Phys. Rev. B **39**, 6636 (1989).

[62]T. Watanabe, T. Takahashi, S. Suzuki, S. Sato, H. Katayama-Yoshida, A. Yamanaka, F. Minami, and S. Takekawa, Physica C **176**, 274 (1991).

[63]C. G. Olson, R. Liu, D. W. Lynch, R. S. List, A. J. Arko, B. W, Veal, Y. C. Chang, P. Z. Jiang, and A. P. Paulikas, Phys. Rev. B **42**, 381 (1990).

[64]R. Claessen, R. Manzke, H. Carstensen, B. Burandt, T. Buslaps, M. Skibowski, and J. Fink, Phys. Rev. B **39**, 7316 (1989).

[65]H. Krakauer and W. E. Pickett, Phys. Rev. Lett. **60**, 1665 (1988).

[66]M. S. Hybertsen and L. F. Mattheiss, Phys. Rev. Lett. **60**, 1661 (1988).

[67]F. Herman, R. V. Kasowski, and W. Y. Hsu, Phys. Rev. B **38**, 204 (1988).

[68]P. Kuiper, M. Grioni, G. A. Sawatzky, D. B. Mitzi, A. Kapitulnik, A. Santaniello, P. de Padova, and P. Thiry, Physica C **157**, 260 (1989).

[69]F. J. Himpsel, G. V. Chandrashekhar, A. B. McLean, and M. W. Shafer, Phys. Rev. B **38**, 11 946 (1988).

[70]T. Timusk and D. B. Tanner, in *Physical Properties of High Temperature Superconductors I,* edited by D. M. Ginsberg (World Scientific, Singapore, 1989), p. 339.

[71]G. A. Thomas, J. Orenstein, D. H. Rapkine, M. Capizzi, A. J. Millis, L. F. Schneemeyer, and J. V. Wasczak, Phys. Rev. Lett. **61**, 1313 (1988).

[72]R. T. Collins, Z. Schlesinger, F. Holtzberg, P. Chaudhari, and C. Feild, Phys. Rev. B **39**, 6571 (1989).

[73]M. Grilli, R. Raimondi, C. Castellani, C. Di Castro, and G. Kotliar, Phys. Rev. Lett. **67**, 259 (1991); Int. J. Mod. Phys. B **5**, 309 (1991).

[74]B. G. Vekhter, Chem. Phys. Lett. **176**, 67 (1991).

[75]D. I. Khomskiĭ and E. I. Neimark, Physica C **173**, 342 (1991).

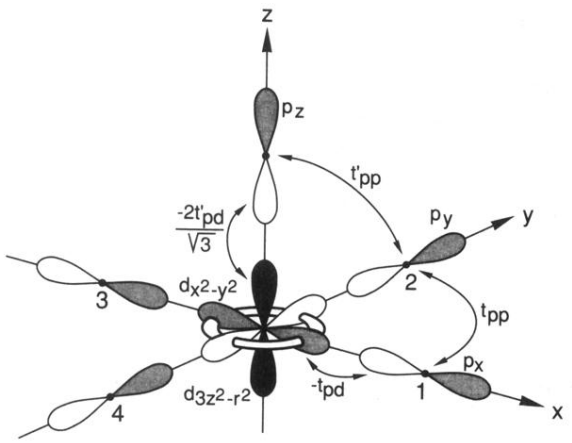

FIG. 1. Orbitals and phase convention (shaded lobes have positive sign) entering the five-band model; a unit cell contains the Cu ion, the planar-oxygen ions 1 and 2, and the apical oxygen(s).